



**HAL**  
open science

# Unravelling physiological signatures of tomato bacterial wilt and xylem metabolites exploited by *Ralstonia solanacearum*

Léo Gerlin, Antoine Escourrou, Cédric Cassan, Felicià Maviane Macia, Nemo Peeters, Stéphane Genin, Caroline Baroukh

## ► To cite this version:

Léo Gerlin, Antoine Escourrou, Cédric Cassan, Felicià Maviane Macia, Nemo Peeters, et al.. Unravelling physiological signatures of tomato bacterial wilt and xylem metabolites exploited by *Ralstonia solanacearum*. *Environmental Microbiology*, 2021, 23 (10), pp.5962-5978. 10.1111/1462-2920.15535 . hal-03211148

HAL Id: hal-03211148

<https://hal.inrae.fr/hal-03211148>

Submitted on 21 May 2021

**HAL** is a multi-disciplinary open access archive for the deposit and dissemination of scientific research documents, whether they are published or not. The documents may come from teaching and research institutions in France or abroad, or from public or private research centers.

L'archive ouverte pluridisciplinaire **HAL**, est destinée au dépôt et à la diffusion de documents scientifiques de niveau recherche, publiés ou non, émanant des établissements d'enseignement et de recherche français ou étrangers, des laboratoires publics ou privés.



Distributed under a Creative Commons Attribution 4.0 International License

1 **Unravelling physiological signatures of tomato bacterial wilt and xylem**  
2 **metabolites exploited by *Ralstonia solanacearum***

3 Léo Gerlin<sup>1</sup>, Antoine Escourrou<sup>1</sup>, Cédric Cassan<sup>2,3</sup>, Felicià Maviane Macia<sup>1,4</sup>, Nemo Peeters<sup>1,4</sup>,  
4 Stéphane Genin<sup>1\*</sup>, Caroline Baroukh<sup>1\*</sup>

5

6 <sup>1</sup>LIPM, Université de Toulouse, INRAE, CNRS, Castanet-Tolosan, France

7 <sup>2</sup>UMR BFP, Université de Bordeaux, INRAE, 33882 Villenave d'Ornon, France

8 <sup>3</sup>Bordeaux Metabolome, MetaboHUB, PHENOME-EMPHASIS, 33140 Villenave d'Ornon, France

9 <sup>4</sup>Toulouse-Plant-Microbe-Phenotyping TPMP PHENOTOUL PHENOME-EMPHASIS LIPM,  
10 Université de Toulouse, INRAE, CNRS, Castanet-Tolosan, France

11 \*For correspondence:

12 Postal address: Caroline Baroukh, Laboratoire des Interactions Plantes-Microorganismes, 24 chemin de Borde Rouge –  
13 Auzeville, CS 52627, 31326 CASTANET TOLOSAN CEDEX, France

14 Email: [caroline.baroukh@inrae.fr](mailto:caroline.baroukh@inrae.fr);

15 Tel.: (+33) 5 61 28 55 25;

16

17 Keywords: metabolism, plant pathogen, transpiration, growth, glutamine, putrescine, NMR,  
18 metabolomics, automated phenotyping

19 Running title: Xylem metabolites exploited during bacterial wilt

20 **Originality-Significance Statement.**

21 The plant pathogen *Ralstonia solanacearum* colonizes plant xylem vessels, reaching  $10^{10}$  colonies per  
22 gram of plant. To proliferate so dramatically and thwart host responses, the nutritive resource supply  
23 is central to successful infection, but is still poorly understood. Through a combination of automated  
24 phenotyping, quantitative metabolomics and genetic approaches, we identify on the one hand sensitive  
25 markers of the infectious process and on the other hand nutritional substrates that allow the rapid  
26 growth of the pathogen in vascular tissues. In particular, we show that during bacterial colonization,  
27 xylem is depleted in two amino acids abundantly present: glutamine and asparagine. In addition, we  
28 show that sugars have little role to sustain growth of the pathogen and progression of the disease, using  
29 a mutant unable to catabolize glucose, sucrose and fructose. These findings challenge the classical  
30 view that the pathogen's infection process depends on abundant sugars in plants to colonize xylem.  
31 Furthermore, the monitoring of plant physiological markers during infection reveals that the phase of  
32 amino acid assimilation and simultaneous bacterial proliferation corresponds to a tipping point of the  
33 infection, associated with a strong alteration of plant physiology including growth arrest and  
34 transpiration arrest.

35

## 36 **Summary**

37 The plant pathogen *Ralstonia solanacearum* uses plant resources to intensely proliferate in xylem  
38 vessels and provoke plant wilting. We combined automatic phenotyping and tissue/xylem quantitative  
39 metabolomics of infected tomato plants to decipher the dynamics of bacterial wilt. Daily acquisition  
40 of physiological parameters such as transpiration and growth were performed. Measurements allowed  
41 us to identify a tipping point in bacterial wilt dynamics. At this tipping point, the reached bacterial  
42 density brutally disrupts plant physiology and rapidly induces its death. We compared the metabolic  
43 and physiological signatures of the infection to drought stress, and found that similar changes occur.  
44 Quantitative dynamics of xylem content enabled us to identify glutamine (and asparagine) as primary  
45 resources *R. solanacearum* consumed during its colonization phase. An abundant production of  
46 putrescine was also observed during the infection process and was strongly correlated with *in planta*  
47 bacterial growth. Dynamic profiling of xylem metabolites confirmed that glutamine is the favored  
48 substrate of *R. solanacearum*. On the other hand, a triple mutant strain unable to metabolize glucose,  
49 sucrose and fructose appears to be only weakly reduced for *in planta* growth and pathogenicity.

50

## 51 **Introduction**

52 The *Ralstonia solanacearum* species complex (RSSC) includes a diverse group of pathogenic strains,  
53 causative agents of bacterial wilt on many plants (Álvarez et al., 2010; Hayward, 1991). These strains  
54 were classified in four main evolutionary lineages also called phylotypes (Fegan & Prior, 2005) which  
55 were recently assigned to three distinct species (Prior et al., 2016; Safni et al., 2014). The bacterial wilt  
56 disease caused by RSSC strains on tomato results from a multi-stage infection process in which, after  
57 the root infection stage and colonization of the root cortex tissues, bacteria invade the xylem vessels.  
58 This allows their spread to the aerial part of the plant, concomitantly with a strong multiplication  
59 (Caldwell et al., 2017; Vasse et al., 1995; Xue et al., 2020). High population density in the xylem  
60 vessels, along with the production of exopolysaccharide (EPS), reduces the sap flow leading to the  
61 appearance of wilting symptoms (Hikichi et al., 2017). Resistance of the plant to limit bacterial  
62 colonization proceeds at different steps including root invasion (Morel, Guinard, et al., 2018;  
63 Poueymiro et al., 2009), vertical movement upwards to the stem, and vessel to vessel diffusion in the  
64 xylem (Caldwell et al., 2017; Planas-Marquès et al., 2020; Xue et al., 2020). On the other hand, *R.*  
65 *solanacearum* spp. relies on effectors delivered by the type-three secretion system to circumvent plant  
66 immunity (Landry et al., 2020) as well as many other virulence factors which contribute to pathogenic  
67 fitness at the different infection steps (Genin & Denny, 2012; Hikichi et al., 2017).

68 Once in xylem vessels, *R. solanacearum* spp. reaches massive bacterial density up to  $10^{10}$  colony  
69 forming units (CFU) per g of fresh stem (Lowe-Power, Khokhani, et al., 2018; Perrier et al., 2019).  
70 Therefore, bacterial infection success is highly dependent on the rapid assimilation of nutrients to  
71 sustain both production of biomass (proliferation) and factors subverting host immunity (virulence)  
72 (Lowe-Power, Khokhani, et al., 2018). There is evidence for intertwined regulation between virulence  
73 genes and metabolic genes (Khokhani et al., 2017; Peyraud et al., 2016, 2018), but how metabolic  
74 resources are acquired *in planta* remains poorly understood. A recent study, however, showed that sap

75 from infected plants is enriched in several nutrients that improve *R. solanacearum* growth in sap  
76 (Lowe-Power, Khokhani, et al., 2018), notably sucrose (Hamilton et al., 2021).

77 The consumption of host resources associated with intense bacterial proliferation, as well as the effects  
78 of virulence factors, should induce strong alterations of the plant physiology. In the case of bacterial  
79 wilt, only qualitative observations of wilting are usually made, and little is known about these  
80 physiological alterations in terms of dynamic and quantitative data. The progression of the disease is  
81 generally evaluated by a disease index (i.e a visual scoring of the wilting symptoms) or by counting of  
82 the bacterial population extracted from infected plants. Although the latter method appears more  
83 sensitive for monitoring the course of the disease, it sometimes happens that the bacterial load is not  
84 correlated with disease symptom progression (Angot et al., 2006; Lebeau et al., 2011).

85 In this study, we aimed at quantifying the dynamics of the bacterial wilt disease on tomato plants in  
86 greenhouse conditions, using *Ralstonia pseudosolanacearum* GMI1000 (Salanoubat et al., 2002), a  
87 model strain representative of the RSSC. We used automated plant phenotyping and metabolomics of  
88 both xylem sap and plant organs to determine the evolution of various physiological parameters at  
89 different stages of xylem vessels colonization. This quantitative kinetic study unraveled a critical point  
90 in the *R. solanacearum* colonization process beyond which the host-pathogen interaction switches to  
91 the side of the disease, with strong physiological effects on the plant and a rapid progression of  
92 symptoms. In a 48h window after infection, the pathogen drains the major substrates allowing for its  
93 strong proliferation. Quantitative metabolomics of infected xylem confirmed that putrescine  
94 concentration is a relevant marker of the infection process and strongly suggested that glutamine and  
95 asparagine are the major carbon sources sustaining bacterial proliferation *in planta*. On the other hand,  
96 the generation of a triple mutant strain defective for the assimilation of glucose, sucrose and fructose  
97 revealed that these sugars play little role in sustaining pathogen's growth *in planta*, as evidenced by  
98 the phenotype of this strain on tomato plants.

99

## 100 **Results**

### 101 **High-throughput phenotyping of tomato plants during bacterial wilt**

102 To evaluate the physiological and metabolic parameters associated with the infection of *R.*  
103 *solanacearum* strain GMI1000 of its tomato host, we monitored the progression of the bacterial wilt  
104 symptoms over 9 days in a controlled conditions greenhouse using an automated high-throughput plant  
105 phenotyping facility (<http://tpmp.inrae.fr>). To improve the synchronization of plant infection, the  
106 inoculation was carried out on root-damaged plants by soil drenching with a suspension of  $5.10^6$   
107 CFU/ml. Control plants (hereafter referred to as ‘healthy plants’) were inoculated with water only.  
108 Two independent experiments comprising respectively 90 and 81 plants were performed. Each  
109 experiment was analyzed separately (automatic phenotyping, metabolomics) and a similar response  
110 profile was observed for both. The data presented in the following sections correspond to an  
111 experiment (three replicates, 81 plants with 63 infected / 18 healthy); the data of the second experiment  
112 are presented in Fig. S4, Fig. S6, Table S1. A larger number of infected plants was monitored given  
113 the greater variability expected in the case of the interaction with the pathogen. Automated  
114 phenotyping included weighing for the estimation of transpiration and imaging. Analysis of acquired  
115 images (Fig. S1) allowed to estimate the position (vertical) of the plant center of gravity (Fig. S2 and  
116 Fig. S3) and the chlorophyll content (Liang et al., 2017). Plants were also manually sampled at different  
117 days post inoculation (1, 3, 4, 5, 7, 8) to determine organ fresh/dry weight, as well as organ and xylem  
118 biochemical profiling and bacterial population (CFU). The appearance of bacterial wilt symptoms,  
119 from 0 (no symptoms) to 4 (complete wilting) (Arlat & Boucher, 1991) was also followed.

120

### 121 ***R. solanacearum* alters the plant physiological balance rapidly after infection**

122

123 *Figure 1*

124 Physiological dynamics of the disease progression clearly revealed a tipping point in plant physiology  
125 and infection kinetic. In our experimental conditions, this point is at 4 dpi and corresponds to a  
126 colonization stage of  $10^8$  bacterial colonies per g of FW (Figure 1). Before this tipping point, plant  
127 general physiology remains similar between healthy and infected individuals: growth/transpiration  
128 rates, chlorophyll content/center of gravity vertical position estimation (Figure 1, Figure 2). At 4 dpi,  
129 transpiration begins to decrease significantly for infected plants, indicating that bacterial colonization  
130 is starting to affect plant physiology in a detectable way, although symptoms are barely visible (50%  
131 of plants at disease index 0). Early impact on transpiration was expected as xylem occlusion limits the  
132 transmission of water to aerial parts. This very early stage of symptom development shows that before  
133 disease index score 2 the plant has already been strongly colonized by bacteria. Position of the plant  
134 center of gravity, which is a proxy of how upwards the plant is growing, is also significantly affected  
135 (Figure 2) at 4 dpi. Some physiology parameters such as plant growth and chlorophyll content were  
136 impacted later and correlated with disease symptom appearance (disease index of 1 and above). From  
137 5 dpi only, plant growth began to slow down for infected plants and chlorophyll content started to  
138 decrease, further showing that a major transition occurred around 4 dpi. We will refer below to this  
139 major transition as the “tipping point”.

140 After this tipping point, infected plants almost stopped growing: the growth rate was  $0.044 \text{ d}^{-1}$  for  
141 infected plant versus  $0.2126 \text{ d}^{-1}$  for healthy plants between 4 and 8 dpi. Transpiration also strongly  
142 decreased, from nearly 100 mL to less than 10 mL per day, while it reached around 200 mL per day  
143 for larger healthy plants. Furthermore, the fastest bacterial proliferation was observed around the  
144 tipping point (bacterial growth rate of  $0.09 \text{ h}^{-1}$  between 3 and 5 dpi), before slowing down (bacterial  
145 growth rate of  $0.02 \text{ h}^{-1}$  between 5 and 8 dpi). It indicated that the first colonization stage in xylem  
146 vessels is a fast proliferation of *R. solanacearum* with limited visible impacts (symptoms) but which  
147 induces a major shift in plant physiology. After this shift, bacterial proliferation slows down as the

148 high-density population of the pathogen begins to become a burden to plant development. This is  
149 probably due to lack of nutrients because of plant stopped growth.

150 *Figure 2*

### 151 **Tomato organ-specific changes induced by the bacterial wilt disease**

152 Fresh and dry weights of healthy and infected plant organs were used to determine the impact of *R.*  
153 *solanacearum* proliferation on plant water status (Figure 3A). Organ water content remains constant  
154 for healthy plants. As expected from our transpiration results (Figure 1), the percentage of water in  
155 infected plants decreased during bacterial infection for leaves and stems. Organ dehydration was  
156 observed close to the previously defined tipping point (a detachment is observed at 4 dpi, although it  
157 is significant only at 5 dpi), almost simultaneously to the onset of transpiration deficiency (as observed  
158 in Figure 1), and close to the appearance of wilting symptoms (disease index). For roots, water content  
159 was in a similar range for infected and healthy plants, confirming that major bacterial proliferation in  
160 xylem vessels does not affect root hydration (Lowe-Power, Khokhani, et al., 2018). At later infection  
161 stage (7 and 8 dpi), corresponding to a disease index score of 3 (75% of the plant wilted) with plant  
162 transpiration close to 0 mL/day, leaves and stems remained however well-hydrated, only decreasing  
163 from 87% to 80% water and 95% to 92%, respectively.

164 Plant dehydration is suspected to affect central metabolism as high-water supply is essential for  
165 photosynthesis as well as for plant development/growth since water is necessary to constitute the turgor  
166 pressor. We thus performed quantitative metabolomics of plant tissues at 3, 5 and 7 dpi (Figure 3B,  
167 Fig. S5), to analyze different steps of the infection process. We did not find significant differences at  
168 3 and 5 dpi. At 7 dpi, a drastic and significant impact on leaf and stem starch was observed (Figure  
169 3B). In leaves, the proportion of starch was high in healthy plants ( $8.58 \pm 6.06$  %) while it was depleted  
170 in infected plants ( $0.08 \pm 0.12$  %). Amino acids also decreased significantly but less drastically. In  
171 accordance with the chlorophyll drop as deduced from image analysis (Figure 2), the quantification of  
172 chlorophyll content in leaves also seems to decrease in infected tissues but not significantly.

173 *Figure 3*

174 **The bacterial wilt disease modifies metabolite availability in tomato xylem sap**

175 We investigated further how *R. solanacearum* is able to proliferate intensely in xylem vessels by  
176 determining the carbon sources supporting bacterial proliferation in xylem sap. We extracted xylem  
177 sap of infected and healthy plant at different dpi for quantitative analysis NMR (see Materials and  
178 Methods). To assess which xylem metabolites are affected by infection, we performed a PCA. This  
179 multivariate analysis revealed that two principal components (PCs) explained 65% of the variability  
180 (see Fig. S7), on which we focused our analysis. Each individual point plotted in Figure 4A  
181 corresponds to a xylem sap sample (15 metabolites concentrations) transformed into the two  
182 uncorrelated PCs and associated with the corresponding bacterial population. We found that the first  
183 PC (explaining 30% of the variability) is not correlated with infection stage and reveals an important  
184 variability between plants independent of the infection. However, the second PC (explaining 25% of  
185 the variability) is strongly associated with the bacterial population level. Interestingly, uninfected  
186 xylem samples have very similar metabolic profiles as all the points are clustered whereas infected  
187 samples display a scattered profile. This suggests that impact of bacterial infection on xylem sap  
188 composition is heterogeneous between plants and that there is therefore a certain level of variation at  
189 this stage.

190 We plotted the contribution of the variables (metabolite concentrations) to the two PCs in Figure 4B.  
191 Variables differing most from zero on the horizontal axis (e.g ethanol, lysine, phenylalanine and  
192 valine) have an important contribution to the first PC, which implies that for these compounds there is  
193 an important inter-plant variability not correlated to infection. Conversely, variables differing most  
194 from zero on the vertical axis contribute to the second PC and are therefore associated with the bacterial  
195 population level. High levels of asparagine and glutamine (bottom of the plot) are associated to healthy  
196 plants and plants with low bacterial population, while high levels of putrescine and acetate are

197 associated with high bacterial population (see complete list in Table 1). We found that for healthy  
198 plants, concentrations are constant between 1 and 8 dpi (no statistical differences observed between  
199 sampling days, and no apparent temporal dynamics) so we determined a global mean for each plant  
200 (Table 1, Table S1). Glutamine appeared as the major component of xylem sap (75 percent of molar  
201 organic carbon) whereas the other compounds were found in much lower concentrations (sixteen times  
202 less at least).

203 *Figure 4*

204 *Table 1*

205

206 We found that the progression of the infection was associated with glutamine and asparagine decrease  
207 and provoked the appearance of putrescine (non-detectable in healthy plants) and an increase of acetate  
208 content. We also estimated that aspartate, phenylalanine, lysine, glutamic acid and leucine were not  
209 affected by *R. solanacearum* infection as the absolute loading weights are close to zero (inferior to  
210 0.25). It was difficult to conclude firmly for the other variables as they were in an intermediate (and  
211 so less discriminating) area, between 0.25 and 0.75.

212

### 213 **Dynamic profiling of tomato xylem fluid metabolites during *R. solanacearum* infection**

214 *Figure 5*

215 PCA showed that some tomato xylem metabolites concentration vary during infection by *R.*  
216 *solanacearum*. In order to get a dynamic view of these changes, we monitored metabolite  
217 concentrations over several days in healthy and infected plants. The kinetic data for the 7 compounds  
218 with statistical differences for one time point or more are represented in Figure 5 (and in Fig. S8 for  
219 alanine). We noticed that statistical differences were mostly observed at 3, 4 or 5 dpi, certainly due to

220 a higher number of plants analyzed and sometimes high variability. For additional compounds tested,  
221 no statistical difference was observed (Fig. S8).

222 Putrescine was detected when plant infection resulted in high bacterial proliferation (between 3 and 5  
223 dpi, see Figure 1) and its concentration stabilized in the last days of infection (7 and 8 dpi) when  
224 bacterial multiplication started to slow down. Putrescine therefore appears to be a sensitive and precise  
225 biomarker of the infection: its dynamics is strongly correlated with the onset and evolution of the  
226 bacterial wilt disease. Three other metabolites increase importantly and significantly in infected plants:  
227 3-hydroxybutyric acid increases at 4 and 5 dpi, while it seems to decrease afterward, acetate increases  
228 from 4 to 7 dpi, and alanine (Fig. S8) seems to follow the same pattern than 3-hydroxybutyric acid.

229 Glutamine depletion is striking as the initial concentration (almost 3 mM) decreases to around 1 mM  
230 at the end of the sampling. Simultaneously, asparagine, which is observed at a smaller amount in  
231 healthy plants (around 1.5 mM) is also quickly depleted: our data indicate a drastic drop between 4  
232 and 5 dpi. After this drop, asparagine concentration is around 0 (or at concentrations under the limit of  
233 detection). These parameters prove an intense metabolic activity over a short time window (48 hours)  
234 in xylem vessels, exactly around the tipping point of the infection previously reported (4 dpi).

### 235 **Putrescine production is a reliable marker of *R. solanacearum* infection**

#### 236 *Figure 6*

237 The progression of bacterial wilt disease is usually monitored in two ways: either by disease index  
238 scoring or by enumerating bacteria extracted from infected tissues. We plotted the relationship between  
239 these two phenotypical markers and some of the physiological parameters we monitored during the  
240 infection assay: plant transpiration, putrescine production and glutamine concentration in xylem  
241 (Figure 6). The calculation of the regression coefficients ( $R^2$ ) shows that these three markers are  
242 globally well correlated with the bacterial density (in  $\log_{10}$  CFU/g of fresh weight) and the disease  
243 index, although we observe for the latter a greater dispersion of the points in the early stages of

244 infection. As expected, bacterial population best correlated with wilt symptom development ( $R^2 = 0.81$   
245 with disease index). Plant transpiration is an early marker of infection impact on plant physiology (Fig.  
246 1) and accordingly a clear negative relationship was also observed with the bacterial population rate,  
247 confirming that bacterial proliferation has a strong negative impact on plant transpiration rate. It turned  
248 out that the bacterial population rate in xylem is also well correlated to the metabolic profile of infected  
249 xylem: positive correlation between putrescine concentration (in decimal logarithm) is high ( $R^2=0.66$ ),  
250 indicating that appearance and accumulation of putrescine is directly associated with *R. solanacearum*  
251 infection. Negative correlation with glutamine concentration is also significant but weaker ( $R^2 = 0.54$ ).

252

253 **Genetic evidence that sugars are not major carbon sources supporting growth of *R.***  
254 ***solanacearum* in xylem**

255 *Figure 7*

256 Xylem metabolomics revealed a significant decrease of glutamine over time as well as a negative  
257 correlation between bacterial density and glutamine content, whereas sugar content was found to not  
258 vary. To validate the hypothesis that *R. solanacearum* growth is mostly supported by glutamine and  
259 not sugars, we generated a triple mutant strain unable to uptake (and so metabolize) three major sugars  
260 found in plants: sucrose, glucose and fructose, glucose and sucrose being detected in our xylem content  
261 analysis. The strain GMI1000 glucose transport operon (RSp1632-RSp1635) was identified after  
262 screening a mutant library to identify genes essential for growth on glucose (Peyraud et al., 2018), but  
263 these genes were incorrectly annotated as a xylose transport system. Cumulative deletions in each  
264 sugar transport system were generated to create the mutant strain GRS941. We used *in vitro* growth  
265 assays on microplates to validate that strain GRS941 growth on sucrose (Figure 7A), glucose (Figure  
266 7B) and fructose (Fig. S9) was severely impacted. We then performed automated phenotyping of strain  
267 GRS941 on tomato plants under conditions similar to those used for the wild-type strain. We observed

268 that growth *in planta* of strain GRS941 was similar to the wild-type and reached high population levels  
269 (Figure 7C). The transpiration rate was significantly lower for plants infected by GRS941 compared  
270 to the wild-type at 6 to 8 dpi, but the difference was small with a similar overall profile and an identical  
271 tipping point at 4 dpi (Figure 7D). Small but statistically significant variations of plant dry weight,  
272 disease index and imaging profiles were also observed (Figure 7, Fig. S9), but the mutant strain was  
273 still able to provoke full plant wilting symptoms. We therefore concluded that glucose, fructose and  
274 sucrose are not critical carbon sources sustaining the pathogen growth during the xylem infection stage,  
275 but rather complementary nutritive sources..

## 276 **Discussion**

277 In this study, we followed the dynamics of infection of the pathogen at the time of xylem colonization  
278 and its impact on plant physiology. Unlike several studies that have focused on the *R. solanacearum*-  
279 plant interaction using miniaturized in vitro pathosystems, we have conducted this work on 4-week  
280 old tomato plants grown in greenhouse conditions to get closer to *in natura* interactions. In order to  
281 synchronize the infection process, we carried out infections with scarified roots, enabling easier entry  
282 of bacteria into vascular tissues. This root wounding procedure made it possible to follow the infection  
283 kinetics with relatively homogeneous values of the measured parameters (see Figure 1, 2, 3, 5),  
284 contrary to what is observed with soil soaking inoculations where greater variability is observed  
285 (Morel, Peeters, et al., 2018). We used our experimental system to follow not only symptoms but also  
286 general growth and water status of the plant, as well as measure metabolites without a priori. We were  
287 then able for the first time to correlate them in a time series for a finer understanding of the overall  
288 process.

289

### 290 **Physiological markers define a tipping point during of bacterial wilt infection.**

291 The use of automated phenotyping has enabled us to collect many measurement points, thus allowing  
292 for a sensitive estimation of major parameters linked to the infection of tomato by *Ralstonia*  
293 *pseudosolanacearum*. In particular, our study reveals that markers such as the plant transpiration rate  
294 in plant tissue are excellent proxies to follow the progression of bacterial infection. Moreover, the  
295 comparison of the measurements in these standardized conditions show that the quantification of the  
296 bacterial load in planta, despite being destructive, is much more reliable than the rating of the  
297 symptoms by disease index which is still commonly used to follow the evolution of an infection (see  
298 Figure 6). The absence of visible symptoms is observed with plants already highly infected (up to  $10^9$   
299 CFU per g of FW) and disease index scores of 0, 1 and 2 include very diverse *in planta* bacterial loads.

300 It is only when the disease index reaches 3 that the profiles become more homogeneous, but they  
301 correspond to an already very advanced stage of bacterial propagation and alteration of plant  
302 physiology. This emphasizes that disease index is a late marker of the infection process and some  
303 physiological markers such as the plant transpiration rate or vertical position of the center of gravity  
304 (proxy of how upwards the plant is growing) have a much better correlation with bacterial colonization.

305 The fine tracking of parameters (weight, transpiration, center of gravity, chlorophyll content) of the  
306 infection highlighted a specific step that we consider a tipping point beyond which the disease  
307 progresses to plant death. This tipping point corresponds to a stage where macroscopic disease  
308 symptoms are barely visible (disease index=0.5) and to the first detection of bacteria after extraction  
309 from plant tissues for counting (CFU per g of FW). This reveals that the plant can afford a load of  
310 bacteria in its vascular system before seeing its immunity overwhelmed by the pathogen, which is  
311 consistent with the observation of bacterial proliferation reaching  $10^6$  CFU per g of fresh weight in the  
312 resistant tomato plant cultivar Hawaii 7996 (Nakaho et al., 2004). We assume that the dynamics around  
313 a tipping point described here is a conserved trait of bacterial wilt, however its temporal positioning  
314 could vary depending on the plant species and plant age (which could influence immune response or  
315 root infection).

316 The plant water loss observed during *R. solanacearum* infection (Figure 3) is in a similar range to that  
317 observed during drought on tomato (Sánchez-Rodríguez et al., 2010), around 10% of water content,  
318 showing that bacterial wilt imposes significant drought stress on the plant. Photosynthesis requires a  
319 big amount of water, so water deficit should quickly impair photosynthesis and, therefore, have an  
320 impact on the ability to store carbon such as starch during the daytime phase of the day. In agreement  
321 with this, we observed in our metabolomic analysis a clear drop in starch storage in infected aerial  
322 parts at 7 dpi (Figure 3). The estimation of chlorophyll content by imaging revealed a progressive  
323 decrease after infection, which remained limited at 7 dpi (Figure 3). The incidence of bacterial wilt is  
324 probably less apparent on the chlorophyll content than on the accumulation of starch since chlorophyll,

325 even though described as decreasing under stress, is subjected to a turnover slower than starch  
326 (Scialdone et al., 2013).

327

### 328 **Quantitative insights in *R. solanacearum* preferred carbon sources in xylem.**

329 In a second part of this work, we studied the kinetic variations of metabolites of xylem sap associated  
330 with the bacterial wilt disease. The fast proliferation of *Ralstonia* spp in xylem must be sustained by  
331 nutrients that the pathogen uptakes in this environment. We therefore studied specifically the  
332 metabolites that were less abundant in the sap of infected plants compared to that of healthy plants,  
333 presumably used by bacteria for efficient growth. The PCA multivariate analysis of metabolomic data  
334 revealed that glutamine and asparagine are significantly depleted in infected plants. This is particularly  
335 striking for glutamine for which the initial concentration ( $2.66 \pm 1.34$  mM at 1 dpi) decreases to lower  
336 than 1 mM at the last days of sampling. Glutamine is described as the major organic component of  
337 xylem sap in plants of different botanical families (Andersen & Brodbeck, 1989; Montes Borrego,  
338 Miguel; Jiménez-Díaz et al., 2017; Zuluaga et al., 2013). Our data are in line with these reports:  
339 glutamine in tomato xylem sap was measured  $3.29 \pm 1.25$  mM for non-infected plants, which  
340 represents 75% of the molar organic carbon in this compartment. We showed that glutamine  
341 concentration was negatively correlated with bacterial growth, supporting the view that glutamine is  
342 most probably the main carbon source sustaining fast proliferation in vascular tissues. As glutamine is  
343 by far the most abundant amino acid in xylem, we hypothesize that *R. solanacearum* has adapted to  
344 preferentially metabolize this compound. The five different transport systems for this compound  
345 present in the genome of GMI1000 highlight the high importance of this metabolite.

346 Simultaneously to glutamine, the asparagine pool (around  $0.178 \pm 0.074$  mM in sap of healthy plants)  
347 is quickly depleted after 4 dpi, falling under the detection limit (between 1  $\mu$ M and 10  $\mu$ M). According  
348 to our data, sugars do not appear to play a major role as sources of energy supply for the bacteria in

349 xylem vessels. Indeed, sugars are present in scarce proportions compared to amino acids such as  
350 glutamine or asparagine. Glucose can be detected but in concentration at the limit of reliable detection,  
351 and the sucrose content also appears rather low. Thus, the sugars concentration does not seem sufficient  
352 to explain the strong bacterial growth. Bacterial infection should lead to the enrichment of the sap with  
353 sugars such as sucrose and glucose, as reported by (Lowe-Power, Hendrich, et al., 2018). However,  
354 based on the kinetic and quantitative values we hypothesized that these metabolites might have a role  
355 in signaling rather than being primary carbon sources to sustain rapid growth, unless sucrose/glucose  
356 dynamics is too fast to be captured by a day by day kinetics. This was confirmed by the behavior of a  
357 triple mutant strain that is unable to grow *in vitro* when glucose, sucrose and fructose are provided as  
358 sole carbon sources. This strain however is still able to colonize the plant, reaching high density in the  
359 stem, and causes physiological alteration in plants (suppression of growth and transpiration) and  
360 symptoms (disease index) delayed but similar to the wild-type strain. We thus concluded that sugars  
361 do not play a major role in the pathogen's growth at this stage.

362 Our metabolomics study also revealed that several potential nutrients (such as aspartate, phenylalanine  
363 and leucine) remain in xylem sap even at later infection stages in concentrations similar to that of  
364 healthy plants. This suggests that these metabolites are not consumed by *R. solanacearum*, probably  
365 due to the lack or non-expression of the appropriate transporter genes. For various other lower  
366 abundant nutrients, the high variability observed in infected plants prevents making clear conclusions.  
367 In an earlier study, Zuluaga et al. (2013) analyzed the xylem sap content of tomato and it should be  
368 noted that some carbon sources reported in their study were not detected in ours. This mainly concerns  
369 amino acids such as GABA (gamma-aminobutyric acid), histidine and serine. The presence of fructose  
370 was also detected while our data reveal the presence of sucrose but not fructose. Higher quantities of  
371 glucose, fructose and sucrose were found in the tomato apoplast (Zuluaga et al., 2013). However, as  
372 the GRS491 triple mutant strain was still able to cause effective bacterial wilt, this suggests that

373 metabolization of these sugars is also not essential for the growth of *R. solanacearum* in the apoplastic  
374 environment.

375 A recent study revealed glutamic acid as a major amino acid promoting expression of some *R.*  
376 *solanacearum* pathogenic traits (Shen et al. 2020) . Inversely to glutamine, glutamic acid is present in  
377 trace amounts in our xylem sap analysis (Table 1) and its concentration remains constant during  
378 infection. The NMR analysis of xylem sap unambiguously discriminated between the two amino acids  
379 (Fig. S10). Therefore, we favor a role of glutamic acid in signaling to induce production of virulence  
380 factors rather than as a major carbon source metabolized in xylem vessels.

381

### 382 **Metabolic signatures of bacterial wilt.**

383 Beside the depletion of some metabolites as mentioned above, we also observed the increase of other  
384 compounds in xylem following *R. solanacearum* infection. The emergence of such compounds could  
385 be from bacterial origin (excreted product such as putrescine (Lowe-Power, Hendrich, et al., 2018;  
386 Peyraud et al., 2016)), or part of a plant metabolic response to infection (Zeiss et al., 2019). In some  
387 cases, these compounds could come simultaneously from the bacteria and from the plant. In the case  
388 of putrescine, the role of the molecule may be dual since bacterial production has been shown to  
389 contribute to the wilt symptoms (Lowe-Power, Hendrich, et al., 2018) and also be produced by tomato  
390 cells hijacked by a *Ralstonia spp* TAL effector (Wu et al., 2019).

391 We found that upon infection xylem sap accumulated 3-hydroxybutyric acid, acetate, ethanol and  
392 potentially proline (discriminated by PCA, Figure 4 although no significant difference in the kinetics  
393 on Fig. S8). Accumulation of proline and ethanol has been associated with drought stress (Kelsey et  
394 al., 2014; Sánchez-Rodríguez et al., 2010) and one can assume that the bacterial wilt disease induces  
395 a sudden and brutal water deficit for the infected plant (Zeiss et al., 2019). Ethanol production could  
396 also be a physiological response to xylem occlusion by *R. solanacearum*: the formation of bacterial

397 biofilm would limit the diffusion of oxygen in the xylem vessels, thus inducing a switch to anaerobic  
398 respiration in plant cells and therefore the production of ethanol as a fermentation product. Concerning  
399 proline, its release into the xylem by plant cells may be due to the need to compensate for the depletion  
400 of glutamine / asparagine consumed by the bacteria. Acetate was also found to appear in infected  
401 xylem; similarly to ethanol, acetate could be a plant fermentation product due to a limitation of oxygen  
402 diffusion, but it could also result from an overflow of the bacterial metabolism (El-Mansi & Holms,  
403 1989). As previously reported by Lowe-Power et al. (2018), we observed an increased synthesis of 3-  
404 hydroxybutyric acid. 3-hydroxybutyric acid is a precursor of PHB (polyhydroxybutyrate), a storage  
405 polymer identified in *R. solanacearum* and phylogenetically close  $\beta$ -proteobacteria. Kinetics showed  
406 an increase followed by a decrease phase of 3-hydroxybutyric acid concentration (Figure 4C), in  
407 agreement with the hypothesis that this metabolite could be excreted by *Ralstonia* and then consumed  
408 before returning to the soil (Lowe-Power et al., 2018). However, it cannot be excluded that bacteria  
409 induce production of 3-hydroxybutyric acid by the plant, as the biosynthetic pathway is present in  
410 tomato plant (Yuan et al., 2016).

411 In a complementary approach, Lowe-Power and collaborators (2018) have recently performed GC-  
412 MS metabolomics of tomato xylem sap infected by *R. solanacearum*. This allowed a non-targeted  
413 approach but not an absolute quantification of the metabolites as we were able to achieve it by the  
414 NMR approach. Based on the relative fold-change of metabolites in the xylem sap of healthy versus  
415 infected plants, several carbon sources such as galactose, 3-hydroxybutyrate, gluconate and glucose  
416 were identified as important carbon sources for *R. solanacearum* in the xylem (Lowe-Power, Hendrich,  
417 et al., 2018). In our study, except for 3-hydroxybutyric acid and glucose (at a concentration below 0.1  
418 mM), the other compounds were not detected, indicating that these compounds are in concentration  
419 below 1 – 10  $\mu$ M, which is the sensibility limit of NMR. Significant change folds can be observed  
420 more easily for low-concentration metabolites than for abundant ones. This thus suggests that the  
421 metabolites, even if they had high fold change, are probably not primary carbon sources supporting

422 bacterial growth. Given the quantities of carbon source available in tomato xylem sap and their  
423 observed consumption by *R. solanacearum* (Figure 5), the most likely hypothesis is that co-  
424 consumption of glutamine and asparagine is the main means used by the pathogen to support its high  
425 proliferation in xylem. The redundancy observed in the genome at the level of glutamine transporter  
426 genes (five unlinked loci identified) reinforces the view that this amino acid is probably crucial to the  
427 *R. solanacearum* fitness inside the plant vascular system.

## 428 **Experimental procedures**

### 429 **Plant cultures and automatic phenotyping**

430 Two independent experiments were conducted for this study. In both cases, tomato seeds (*Solanum*  
431 *lycopersicum* M82) were grown in soil (SB2, Proveen, The Netherlands) supplemented with  
432 Osmocote® coated fertilizer at a rate of 4g/L. Seed were germinated in a growth chamber (26°C, 67%  
433 HR, 12h- LED light per day). Around a hundred of plantlets were transplanted in individual plastic  
434 pots (8x8cm) 8 days after sowing. 16 days after sowing, 90 young plants were chosen and repotted in  
435 3L pots until the end of the experiment. Foam cover discs were placed on each pot to limit the  
436 evaporation.

437 On the first experiment, 90 plants were loaded on the Phenoserre robot facility of the Toulouse Plant  
438 Microbe Phenotyping infrastructure, of which 45 plants were inoculated with *R. pseudosolanacearum*  
439 GMI1000 strain (Salanoubat et al., 2002) and another 45 mock-inoculated with sterile water (referred  
440 to as “Healthy plants”). 12h-light per day at 28°C and 50% humidity were programmed. On the second  
441 experiment, 81 plants were loaded on the Phenoserre robot, of which 63 infected and 18 healthy plants.

442 All the plants were watered with 100 ml three times on the loading day and weighted, in order to define  
443 a well-watered target weight. The subsequent watering was conducted automatically once a day to the  
444 target weight. Imaging was programmed four times a day (starts at 2.00 a.m., 9.00 a.m., 4.30 p.m, and  
445 7.30 p.m, for a total duration of around one hour and a half per imaging job), the conveyor belt bringing  
446 the individual plants to a side-RGB camera. The plants were then automatically weighted after each  
447 imaging session. The daily transpiration was determined as the weight differences between two  
448 consecutive days, at the time of watering. Temperature, hygrometry and light intensity were recorded  
449 during the whole experiment.

### 450 **Plant image analysis**

451 Fig. S1 presents the step-by-step segmentation performed using a set of python algorithms allowing  
452 for the testing of the segmentation pipeline. Every plant is imaged using an RGB camera with a blue  
453 background, under six angles (starting at 0° and then by 60° steps). Three different “Region of Interest”  
454 or ROIs are defined to allow easier analysis, in white containing all the plant information, with a “safe  
455 zone” in green and a “danger zone” in red. As the images are acquired in the exact same conditions,  
456 the ROIs are static. Masks are extracted corresponding to the bulk of the plant (“mask top”), as well  
457 as two additional masks to gather the plant information close to the pot and conveyor (“mask middle”  
458 and “mask bottom”). All three masks are merged in order to build a coarse mask, this latter mask is  
459 then cleaned by removed additional noise to generate a clean mask and allowing for the final features  
460 extraction.

461 Fig S2, displays the “centroid y” (or Cy) morphological traits, which is the y coordinate of the plant  
462 area center of gravity. The origin of the y axe is positioned at the top of the image. A larger Cy value  
463 indicates a center of gravity closer to the pot (further from the top of the image) and is a trait that is  
464 very well associated with the bacterial wilt symptoms, as any “lowering” of the leaves (wilting) has an  
465 impact of the Cy trait. Fig S3 displays some Cy values of plants with different disease index (DI).

#### 466 **Plant inoculation**

467 For both experiments, three replicates of the strain GMI1000 were grown in BG complete medium  
468 (Plener et al., 2010) at 28°C. Bacterial cells were washed, resuspended in sterile water and each plant  
469 was inoculated with one of the three replicates by pouring 50 ml of a suspension at  $5 \cdot 10^6$  CFU/ml at  
470 the stem base 4 days after the loading on the robot. Just before inoculation, roots were scarified with a  
471 scalpel blade in order to synchronize the infection rate.

#### 472 **Collection and preparation of plant samples**

473 For the first experiment, plants were removed each day from the conveyor belt for samplings during 9  
474 consecutive days. On the inoculation day and at 7 and 8 dpi, 3 healthy and 3 infected plants were

475 removed. From 2 to 6 dpi, 6 healthy and 6 infected plants were removed each day. For the second  
476 experiment, plants were removed from the conveyor belts for samplings at 1, 3, 4, 5, 7 and 8 dpi. Each  
477 sampling day, 3 healthy plants and respectively, 3, 6, 14, 16, 14, 10 infected plant were removed.

478 In both experiments, the following procedures were then applied at the same period of the day (between  
479 10 am and 2 pm) to avoid the effect of daily variations in xylem sap/organ chemistry. For the plant  
480 that were removed from the experimental setup, stems were cut just above the cotyledon node, rinsed  
481 with approximately 1 ml of water and the upcoming xylem sap was collected by repeated pipetting  
482 and collection in Eppendorf tubes placed on ice. For the infected plants, the tubes were centrifuged  
483 and the supernatants were transferred in new tubes while the pellets were discarded. The tubes with  
484 xylem sap were placed at -80°C for further quantitative NMR analyses.

485 The different organs of each plant were collected separately (stems, leaves, roots and flowers whenever  
486 they occurred) for fresh and dry weights measurements. Approximately 300 mg fresh weight for each  
487 collected organ was frozen in liquid nitrogen and stored at -20°C for further biochemical analyses.

488 1 cm of stem was sampled above the cotyledons, cut up in small pieces and placed in a 2 ml centrifuge  
489 tube containing glass beads (2 mm diameter) and ground at 30 Hz with a mixer mill (MM 400, Retsch,  
490 Germany) until total grinding (1 to 3 minutes). Extracted bacteria were resuspended in 1 ml of sterile  
491 water, serial-diluted and plated on complete BG medium supplemented with triphenyl tetrazolium  
492 chloride, for counting as previously described (Guidot et al., 2014).

493

#### 494 **Quantitative NMR analyses**

495 The xylem saps were analyzed by 1D <sup>1</sup>H NMR on MetaToul analytics platform (UMR5504, UMR792,  
496 CNRS, INRAE, INSA 135 Avenue de Ranguel 31077 Toulouse Cedex 04, France), using the Bruker  
497 Avance 800 MHz equipped with an ATMA 5mm cryoprobe. Each xylem sap sample was centrifuged  
498 to remove the residues (5min, 13520 RCF, Hettich Mikro 200 centrifuge), then placed in 3 mm NMR

499 tubes. TSP-d4 standard (Sodium 3-(trimethylsilyl)(1-<sup>13</sup>C,2H<sub>4</sub>)propanoate), at a final concentration of  
500 100 μM, was used as a reference. pH 6.0 phosphate buffer was used to standardize the chemical shifts  
501 among samples. Acquisition conditions were as follows: 30° pulse angle, 20.0287 ppm spectral width,  
502 64 scans per acquisition for a total scan time of approximately 8 minutes per sample, and zgpr30 water  
503 pre-saturation sequence. The samples were kept at a temperature of 280 K (6.85 °C) all along the  
504 analysis. Resonances of metabolites were manually integrated and the concentrations were calculated  
505 based on the number of equivalent protons for each integrated signal and on the TSP final  
506 concentration. For one equivalent proton, half of the glucose signal was overlapped by the residual  
507 water, as shown on Fig. S10 (around 5.2 ppm). Therefore, its contribution was extrapolated based on  
508 the analysis of a glucose standard.

509

#### 510 **Biochemical analyses of metabolites**

511 Quantifications of metabolites were performed at the HitMe platform (INRAE - IBVM - 71 avenue E.  
512 Bourlaux - CS 20032 - 33882 Villenave d'Ornon Cedex, France). The plants samples, previously  
513 frozen in liquid nitrogen, were ground to a powder using liquid nitrogen to avoid thawing. A quantity  
514 of 20 +/- 10 mg of each were weighted in previously frozen Micronic tubes. Free amino acids, glucose,  
515 fructose, malate, proteins, starch, sucrose and chlorophylls in leaves, stems and roots were quantified  
516 as described in (Biais et al., 2014). Briefly, ethanolic extracts from every samples were obtained using  
517 three consecutive incubation of the frozen ground powder aliquots. Ethanol 80% v/v with  
518 HEPES/KOH 10 mM pH6 buffer was used for the two first incubations, and ethanol 50% v/v with  
519 HEPES/KOH 10 mM pH6 buffer was used for the third. Supernatants were pooled and used for the  
520 quantification of chlorophylls, glucose, fructose, sucrose, malate and free amino acids. Pellets were  
521 used for the determination of protein and starch contents. The extracts and pellets were stored at -20°C  
522 between each quantification. For each sample, chlorophylls were quantified by measuring optical  
523 densities at 645 and 665 nm on a mix of 50 μl of extract supplemented with 150 μl of analytics grade

524 ethanol. Amino acids were quantified using the fluorescamine method. Excitation wavelength was  
525 405nm and emission was measured at 485 nm. The proteins were quantified using Bradford reagent.  
526 Starch was quantified in glucose equivalent after full pellet digestion in an oven at 37°C for 18 hours.  
527 For the other analytes cited above, the NADH/NADPH appearance was measured, and the analytes  
528 were quantified using a 1:1 stoichiometric coefficient.

529 **Generation and phenotyping of *R. solanacearum* triple mutant strain defective for glucose,**  
530 **sucrose and fructose assimilation**

531 Strain GRS941 was engineered by cumulating deletions in the glucose transport operon (RSp1632-  
532 RSp1635), the sucrose assimilation operon (RSp1280-RSp1286) and the fructose transport operon  
533 (RSc2861-RSc2863). Complete procedures for the triple mutant generation are available on Text S1.  
534 For *in vitro* growth assay, preculture on BG complete medium (Plener et al., 2010), cell  
535 centrifugation/washing and resuspension were performed. Strains were then inoculated at an OD (600  
536 nm) of 0.01 on minimal medium (Plener et al., 2010) supplemented with respectively glucose, sucrose,  
537 fructose, glutamine as sole carbon source (at 50 mM of carbon). Growth was assessed using microplate  
538 spectrophotometer (FLUOstar Omega, BMG Labtech, Germany) during 96h at 28°C and under  
539 shaking at 700 rpm. For in planta phenotyping, the same procedure than described for the GMI1000  
540 strain was followed on two independent experiments, with respectively 31 and 41 tomato plants  
541 infected by the mutant strain and similar number of plants infected by the wild-type strain..

542

543

544

545

546 **Supporting Information**

547 Fig. S1. Step-by-step segmentation pipeline.

548 Fig. S2. The Centroid-y trait.

549 Fig. S3. Examples of Cy values on healthy and diseased plants.

550 Fig. S4. Biological replicate of the physiological measurements.

551 Fig. S5. Impact of *R. solanacearum* infection on plant tissues metabolic content.

552 Fig. S6. PCA on the biological replicate data: experimental points (A) and variables (B).

553 Fig. S7. Explained variance of the principal components.

554 Fig. S8. Concentrations profiles for metabolites with non-statistically significant infection effect.

555 Fig. S9. *In vitro* and *in planta* phenotyping of *R. solanacearum* triple mutant strain defective for  
556 glucose, sucrose and fructose assimilation.

557 Fig. S10. NMR spectrum example and spectrum differences between glutamine and glutamic acid (or  
558 glutamate).

559 Table S1. Biological replicate of the composition of non-infected xylem.

560 Table S2. Loading weights on the second component of the PCA.

561 File S1. Script for the segmentation pipeline.

562 Text S1. Generation of *R. solanacearum* triple mutant strain defective for glucose, sucrose and  
563 fructose assimilation.

564

565 **Acknowledgments**

566 LG was funded by a PhD grant from the French Ministry of National Education and Research. AE was  
567 funded by the French Laboratory of Excellence TULIP (ANR-10-LABX-41 and ANR-11-IDEX-0002-  
568 02). The study was funded by the French Laboratory of Excellence (LABEX) project TULIP (ANR-  
569 10-LABX-41 and ANR-11-IDEX-0002-02). The funders had no role in study design, data collection  
570 and analysis, decision to publish, or preparation of the manuscript.

571 We thank TPMP (Toulouse Plant Microbe Phenotyping) platform (Castanet-Tolosan, France) and its  
572 staff Fabrice Devoilles for their technical support in plant cultures and imaging, as well as HiTMe  
573 (High-Throughput Metabolic phenotyping) platform (Villenave d'Ornon, France) for biochemical  
574 analysis of organ metabolites. We acknowledge MetaToul (Metabolomics & Fluxomics Facilities,  
575 Toulouse, France, [www.metatoul.fr](http://www.metatoul.fr)) platform, which is part of the MetaboHUB-ANR-11-INBS-0010  
576 national infrastructure ([www.metabohub.fr](http://www.metabohub.fr)) and its staff Cécilia Berges, Edern Cahoreau and Lindsay  
577 Peyriga for access to NMR facilities. We also thank Patrick Barberis for his expert skills in the  
578 construction of the triple mutant strain.

579 **Author contributions**

580 Conceptualization: SG, CB. Methodology: LG, AE, NP, SG, CB. Formal analysis: LG, AE, FMM,  
581 CB. Investigation: LG, AE, CC, CB. Resources: NP. Writing – Original Draft: LG, AE. Writing –  
582 Review & Editing: LG, AE, NP, SG, CB. Visualization: LG, AE. Project administration: CB. Funding  
583 acquisition: CB.

584 **Data availability statement**

585 All data supporting the findings of this study are available within the paper and within its  
586 supplementary materials published online.

587 **Conflict of interests.** The authors declare no competing interests.

## 588 **References**

- 589 Álvarez, B., Biosca, E. G., & López, M. M. (2010). On the life of *Ralstonia solanacearum*, a  
590 destructive bacterial plant pathogen. *Current Research, Technology and Education Topics in*  
591 *Applied Microbiology and Microbial Biotechnology*, 267–279.  
592 [https://pdfs.semanticscholar.org/aa85/77e213e2977a0e4eb739795e3fea51187181.pdf?\\_ga=2.15](https://pdfs.semanticscholar.org/aa85/77e213e2977a0e4eb739795e3fea51187181.pdf?_ga=2.156465595.1055873898.1504096691-1311319012.1504096691)  
593 [6465595.1055873898.1504096691-1311319012.1504096691](https://pdfs.semanticscholar.org/aa85/77e213e2977a0e4eb739795e3fea51187181.pdf?_ga=2.156465595.1055873898.1504096691-1311319012.1504096691)
- 594 Andersen, P. C., & Brodbeck, B. V. (1989). Diurnal and temporal changes in the chemical profile of  
595 xylem exudate from *Vitis rotundifolia*. *Physiologia Plantarum*, 75(1), 63–70.  
596 <https://doi.org/10.1111/j.1399-3054.1989.tb02064.x>
- 597 Angot, A., Peeters, N., Lechner, E., Vailleau, F., Baud, C., Gentzbittel, L., Sartorel, E., Genschik, P.,  
598 Boucher, C., & Genin, S. (2006). *Ralstonia solanacearum* requires F-box-like domain-  
599 containing type III effectors to promote disease on several host plants. *Proceedings of the*  
600 *National Academy of Sciences of the United States of America*, 103(39), 14620–14625.  
601 <https://doi.org/10.1073/pnas.0509393103>
- 602 Arlat, M., & Boucher, C. (1991). Research Notes Identification of a dsp DNA Region Controlling  
603 Aggressiveness of *Pseudomonas solanacearum*. *Molecular Plant-Microbe Interactions*, 4(2),  
604 211. <https://doi.org/10.1094/mpmi-4-211>
- 605 Biais, B., Bénard, C., Beauvoit, B., Colombié, S., Prodhomme, D., Ménard, G., Bernillon, S., Gehl,  
606 B., Gautier, H., Ballias, P., Mazat, J. P., Sweetlove, L., Génard, M., & Gibon, Y. (2014).  
607 Remarkable reproducibility of enzyme activity profiles in tomato fruits grown under contrasting  
608 environments provides a roadmap for studies of fruit metabolism. *Plant Physiology*, 164(3),  
609 1204–1221. <https://doi.org/10.1104/pp.113.231241>
- 610 Caldwell, D., Kim, B.-S., & Iyer-Pascuzzi, A. S. (2017). *Ralstonia solanacearum* Differentially

- 611 Colonizes Roots of Resistant and Susceptible Tomato Plants. *Phytopathology*, 107(5), 528–536.  
612 <https://doi.org/10.1094/PHYTO-09-16-0353-R>
- 613 El-Mansi, E. M. T., & Holms, W. H. (1989). Control of carbon flux to acetate excretion during  
614 growth of *Escherichia coli* in batch and continuous cultures. *Journal of General Microbiology*,  
615 135(11), 2875–2883. <https://doi.org/10.1099/00221287-135-11-2875>
- 616 Fegan, M., & Prior, P. (2005). How complex is the “*Ralstonia solanacearum* species complex”?  
617 *Bacterial Wilt Disease and the Ralstonia Solanacearum Species Complex*, July, 449–461.
- 618 Genin, S., & Denny, T. P. (2012). Pathogenomics of the *Ralstonia solanacearum* Species Complex.  
619 *Annual Review of Phytopathology*, 50(1), 67–89. [https://doi.org/10.1146/annurev-phyto-](https://doi.org/10.1146/annurev-phyto-081211-173000)  
620 081211-173000
- 621 Guidot, A., Jiang, W., Ferdy, J. B., Thébaud, C., Barberis, P., Gouzy, J., & Genin, S. (2014).  
622 Multihost experimental evolution of the pathogen *ralstonia solanacearum* unveils genes  
623 involved in adaptation to plants. *Molecular Biology and Evolution*, 31(11), 2913–2928.  
624 <https://doi.org/10.1093/molbev/msu229>
- 625 Hamilton, C. D., Steidl, O. R., MacIntyre, A. M., Hendrich, C. G., & Allen, C. (2021). *Ralstonia*  
626 *solanacearum* depends on catabolism of myo-inositol, sucrose, and trehalose for virulence in an  
627 infection stage-dependent manner. *Molecular Plant-Microbe Interactions*®, MPMI-10-20-  
628 0298-R. <https://doi.org/10.1094/MPMI-10-20-0298-R>
- 629 Hayward, A. C. (1991). Biology and Epidemiology of Bacterial Wilt Caused by *Pseudomonas*  
630 *Solanacearum*. *Annual Review of Phytopathology*, 29(1), 65–87.  
631 <https://doi.org/10.1146/annurev.py.29.090191.000433>
- 632 Hikichi, Y., Mori, Y., Ishikawa, S., Hayashi, K., Ohnishi, K., Kiba, A., & Kai, K. (2017). Regulation  
633 Involved in Colonization of Intercellular Spaces of Host Plants in *Ralstonia solanacearum*.

634 *Frontiers in Plant Science*, 8, 967. <https://doi.org/10.3389/fpls.2017.00967>

635 Kelsey, R. G., Gallego, D., Sánchez-García, F. J., & Pajares, J. A. (2014). Ethanol accumulation  
636 during severe drought may signal tree vulnerability to detection and attack by bark beetles.  
637 *Canadian Journal of Forest Research*, 44(6), 554–561. <https://doi.org/10.1139/cjfr-2013-0428>

638 Khokhani, D., Lowe-Power, T. M., Tran, T. M., & Allen, C. (2017). A Single Regulator Mediates  
639 Strategic Switching between Attachment/Spread and Growth/Virulence in the Plant Pathogen  
640 *Ralstonia solanacearum*. *MBio*, 8(5), e00895-17. <https://doi.org/10.1128/mBio.00895-17>

641 Landry, D., González-Fuente, M., Deslandes, L., & Peeters, N. (2020). The large, diverse, and robust  
642 arsenal of *Ralstonia solanacearum* type III effectors and their in planta functions. *Molecular*  
643 *Plant Pathology*, April, 1–12. <https://doi.org/10.1111/mpp.12977>

644 Lebeau, A., Daunay, M. C., Frary, A., Palloix, A., Wang, J. F., Dintinger, J., Chiroleu, F., Wicker,  
645 E., & Prior, P. (2011). Bacterial wilt resistance in tomato, pepper, and eggplant: Genetic  
646 resources respond to diverse strains in the *Ralstonia solanacearum* species complex.  
647 *Phytopathology*, 101(1), 154–165. <https://doi.org/10.1094/PHYTO-02-10-0048>

648 Liang, Y., Urano, D., Liao, K. L., Hedrick, T. L., Gao, Y., & Jones, A. M. (2017). A nondestructive  
649 method to estimate the chlorophyll content of *Arabidopsis* seedlings. *Plant Methods*, 13(1), 26.  
650 <https://doi.org/10.1186/s13007-017-0174-6>

651 Lowe-Power, T. M., Hendrich, C. G., von Roepenack-Lahaye, E., Li, B., Wu, D., Mitra, R., Dalsing,  
652 B. L., Ricca, P., Naidoo, J., Cook, D., Jancewicz, A., Masson, P., Thomma, B., Lahaye, T.,  
653 Michael, A. J., & Allen, C. (2018). Metabolomics of tomato xylem sap during bacterial wilt  
654 reveals *Ralstonia solanacearum* produces abundant putrescine, a metabolite that accelerates wilt  
655 disease. *Environmental Microbiology*, 20(4), 1330–1349. [https://doi.org/10.1111/1462-](https://doi.org/10.1111/1462-2920.14020)  
656 [2920.14020](https://doi.org/10.1111/1462-2920.14020)

657 Lowe-Power, T. M., Khokhani, D., & Allen, C. (2018). How *Ralstonia solanacearum* Exploits and  
658 Thrives in the Flowing Plant Xylem Environment. *Trends in Microbiology*, 26(11), 929–942.  
659 <https://doi.org/10.1016/j.tim.2018.06.002>

660 Montes Borrego, Miguel; Jiménez-Díaz, R. M. ;, Trapero Casas, J. L. ;, Navas Cortés, Juan Antonio ;  
661 Haro, C., Rivas, J. C. ., Fuente, L. de la;, & Landa, B. B. (2017). Metabolomic characterization  
662 of xylem sap of different olive cultivars growing in Spain. *European Conference on Xylella*,  
663 *November*.

664 Morel, A., Guinard, J., Lonjon, F., Sujeeun, L., Barberis, P., Genin, S., Vailleau, F., Daunay, M. C.,  
665 Dintinger, J., Poussier, S., Peeters, N., & Wicker, E. (2018). The eggplant AG91-25 recognizes  
666 the Type III-secreted effector RipAX2 to trigger resistance to bacterial wilt (*Ralstonia*  
667 *solanacearum* species complex). *Molecular Plant Pathology*, 19(11), 2459–2472.  
668 <https://doi.org/10.1111/mpp.12724>

669 Morel, A., Peeters, N., Vailleau, F., Barberis, P., Jiang, G., Berthomé, R., & Guidot, A. (2018). Plant  
670 pathogenicity phenotyping of *Ralstonia solanacearum* strains. In *Methods in Molecular Biology*  
671 (Vol. 1734, pp. 223–239). Humana Press Inc. [https://doi.org/10.1007/978-1-4939-7604-1\\_18](https://doi.org/10.1007/978-1-4939-7604-1_18)

672 Nakaho, K., Inoue, H., Takayama, T., & Miyagawa, H. (2004). Distribution and multiplication of  
673 *Ralstonia solanacearum* in tomato plants with resistance derived from different origins. *Journal*  
674 *of General Plant Pathology*, 70(2), 115–119. <https://doi.org/10.1007/s10327-003-0097-0>

675 Perrier, A., Barlet, X., Rengel, D., Prior, P., Poussier, S., Genin, S., & Guidot, A. (2019).  
676 Spontaneous mutations in a regulatory gene induce phenotypic heterogeneity and adaptation of  
677 *Ralstonia solanacearum* to changing environments. *Environmental Microbiology*, 21(8), 3140–  
678 3152. <https://doi.org/10.1111/1462-2920.14717>

679 Peyraud, R., Cottret, L., Marmiesse, L., & Genin, S. (2018). Control of primary metabolism by a  
680 virulence regulatory network promotes robustness in a plant pathogen. *Nature Communications*,

681 9(1), 418. <https://doi.org/10.1038/s41467-017-02660-4>

682 Peyraud, R., Cottret, L., Marmiesse, L., Gouzy, J., & Genin, S. (2016). A Resource Allocation  
683 Trade-Off between Virulence and Proliferation Drives Metabolic Versatility in the Plant  
684 Pathogen *Ralstonia solanacearum*. *PLoS Pathogens*, *12*(10), e1005939.  
685 <https://doi.org/10.1371/journal.ppat.1005939>

686 Planas-Marquès, M., Kressin, J. P., Kashyap, A., Panthee, D. R., Louws, F. J., Coll, N. S., & Valls,  
687 M. (2020). Four bottlenecks restrict colonization and invasion by the pathogen *Ralstonia*  
688 *solanacearum* in resistant tomato. *Journal of Experimental Botany*, *71*(6), 2157–2171.  
689 <https://doi.org/10.1093/jxb/erz562>

690 Plener, L., Manfredi, P., Valls, M., & Genin, S. (2010). PrhG, a transcriptional regulator responding  
691 to growth conditions, is involved in the control of the type III secretion system regulon in  
692 *Ralstonia solanacearum*. *Journal of Bacteriology*, *192*(4), 1011–1019.  
693 <https://doi.org/10.1128/JB.01189-09>

694 Poueymiro, M., Cunnac, S., Barberis, P., Deslandes, L., Peeters, N., Cazale-Noel, A. C., Boucher, C.,  
695 & Genin, S. (2009). Two type III secretion system effectors from *Ralstonia solanacearum*  
696 GMI1000 determine host-range Specificity on Tobacco. *Molecular Plant-Microbe Interactions*,  
697 *22*(5), 538–550. <https://doi.org/10.1094/MPMI-22-5-0538>

698 Prior, P., Ailloud, F., Dalsing, B. L., Remenant, B., Sanchez, B., & Allen, C. (2016). Genomic and  
699 proteomic evidence supporting the division of the plant pathogen *Ralstonia solanacearum* into  
700 three species. *BMC Genomics*, *17*(1), 1–11. <https://doi.org/10.1186/s12864-016-2413-z>

701 Safni, I., Cleenwerck, I., De Vos, P., Fegan, M., Sly, L., & Kappler, U. (2014). Polyphasic  
702 taxonomic revision of the *Ralstonia solanacearum* species complex: Proposal to emend the  
703 descriptions of *Ralstonia solanacearum* and *Ralstonia syzygii* and reclassify current *R. syzygii*  
704 strains as *Ralstonia syzygii* subsp. *syzygii* subsp. nov., *R. s.* *International Journal of Systematic*

705 *and Evolutionary Microbiology*, 64, 3087–3103. <https://doi.org/10.1099/ijms.0.066712-0>

706 Salanoubat, M., Genin, S., Artiguenave, F., Gouzy, J., Mangenot, S., Arlat, M., Billault, A., Brottiart,  
707 P., Camus, J. C., Cattolico, L., Chandler, M., Choisine, N., Claudel-Renard, C., Cunnac, S.,  
708 Demange, N., Gaspin, C., Lavie, M., Moisan, A., Robert, C., ... Boucher, C. A. (2002).  
709 Genome sequence of the plant pathogen *Ralstonia solanacearum*. *Nature*, 415(6871), 497–502.  
710 <https://doi.org/10.1038/415497a>

711 Sánchez-Rodríguez, E., Rubio-Wilhelmi, Mm., Cervilla, L. M., Blasco, B., Rios, J. J., Rosales, M.  
712 A., Romero, L., & Ruiz, J. M. (2010). Genotypic differences in some physiological parameters  
713 symptomatic for oxidative stress under moderate drought in tomato plants. *Plant Science*,  
714 178(1), 30–40. <https://doi.org/10.1016/j.plantsci.2009.10.001>

715 Scialdone, A., Mugford, S. T., Feike, D., Skeffngton, A., Borrill, P., Graf, A., Smith, A. M., &  
716 Howard, M. (2013). Arabidopsis plants perform arithmetic division to prevent starvation at  
717 night. *ELife*, 2013(2). <https://doi.org/10.7554/eLife.00669>

718 Shen, F., Yin, W., Song, S., Zhang, Z., Ye, P., Zhang, Y., Zhou, J., He, F., Li, P., & Deng, Y. (2020).  
719 *Ralstonia solanacearum* promotes pathogenicity by utilizing <scp>l</scp> -glutamic acid from  
720 host plants. *Molecular Plant Pathology*, 21(8), 1099–1110. <https://doi.org/10.1111/mpp.12963>

721 Vasse, J., Frey, P., & Trigalet, A. (1995). Microscopic studies of intercellular infection and  
722 protoxylem invasion of tomato roots by *Pseudomonas solanacearum*. *Molecular Plant-Microbe*  
723 *Interactions*, 8(2), 241–251. <https://doi.org/10.1094/MPMI-8-0241>

724 Wu, D., von Roepenack-Lahaye, E., Buntru, M., de Lange, O., Schandry, N., Pérez-Quintero, A. L.,  
725 Weinberg, Z., Lowe-Power, T. M., Szurek, B., Michael, A. J., Allen, C., Schillberg, S., &  
726 Lahaye, T. (2019). A Plant Pathogen Type III Effector Protein Subverts Translational  
727 Regulation to Boost Host Polyamine Levels. *Cell Host and Microbe*, 26(5), 638-649.e5.  
728 <https://doi.org/10.1016/j.chom.2019.09.014>

729 Xue, H., Lozano-Durán, R., & Macho, A. P. (2020). Insights into the Root Invasion by the Plant  
730 Pathogenic Bacterium *Ralstonia solanacearum*. *Plants*, 9(4), 516.  
731 <https://doi.org/10.3390/plants9040516>

732 Yuan, H., Cheung, C. Y. M., Poolman, M. G., Hilbers, P. A. J., & van Riel, N. A. W. (2016). A  
733 genome-scale metabolic network reconstruction of tomato (*Solanum lycopersicum* L.) and its  
734 application to photorespiratory metabolism. *The Plant Journal : For Cell and Molecular*  
735 *Biology*, 85(2), 289–304. <https://doi.org/10.1111/tpj.13075>

736 Zeiss, D. R., Mhlongo, M. I., Tugizimana, F., Steenkamp, P. A., & Dubery, I. A. (2019).  
737 Metabolomic Profiling of the Host Response of Tomato (*Solanum lycopersicum*) Following  
738 Infection by *Ralstonia solanacearum*. *International Journal of Molecular Sciences* 2019, Vol.  
739 20, Page 3945, 20(16), 3945. <https://doi.org/10.3390/IJMS20163945>

740 Zuluaga, A. P., Puigvert, M., & Valls, M. (2013). Novel plant inputs influencing *Ralstonia*  
741 *solanacearum* during infection. *Frontiers in Microbiology*, 4(NOV), 349.  
742 <https://doi.org/10.3389/fmicb.2013.00349>

743

744

745 **Figure and table legends**

746 **Table 1. Xylem metabolite content and the impact of *R. solanacearum* infection**

747 1: Effect of infection was deduced from the PCA presented in Figure 4. Metabolite concentration  
748 decrease was assigned for compounds with loading weights on the second component inferior to -0.3  
749 whereas increase in concentration was assigned for those superior to 0.3. Values ranging between -  
750 0.15 and -0.3 correspond to compounds with putative decrease in concentration, those between 0.15  
751 and 0.3 to putative increase. Values ranging from -0.15 and 0.15 defined compounds with no  
752 significant variation in concentration (ie not impacted by infection). Putrescine was considered as  
753 ‘appearing’ as it was absent in healthy plants and had a loading weight on the second component  
754 superior to 0.3. (see Table S2)

755 2: Usage as carbon source (+: growth, -: no growth) was assessed from published Biolog Phenotype  
756 Microarrays data (Peyraud et al., 2016).

757 **Figure 1**

758 Impact of *R. solanacearum* colonization on plant physiology (dry weight/transpiration) and monitoring  
759 of disease kinetics (disease index/bacterial density). The data presented are from an experiment on 81  
760 plants, with at least 3 plants per conditions at each sampling point. Bars indicate standard deviation.  
761 Healthy and infected plant data (transpiration and dry weight) were compared by Wilcoxon-Mann-  
762 Whitney test (\*: p-value<0.05, \*\*: p-value<0.01, \*\*\*\*: p-value <0.0001).

763 **Figure 2**

764 Physiological parameters determined by automatic imaging. Chlorophyll content was estimated  
765 through RGB values of plant images as described by Liang et al (*Liang et al., 2017*). Center of  
766 gravity position (vertical) was estimated through plant imaging with 0 pixel representing the top of  
767 the plant. The data presented are from an experiment on 81 plants with at least 3 plants per  
768 conditions at each sampling point. Bars indicate standard deviation. Healthy and infected plant data

769 were compared by Wilcoxon-Mann-Whitney test (\*: p-value<0.05, \*\*: p-value<0.01, \*\*\*\*: p-value  
770 <0.0001).

771 **Figure 3**

772 Impact of *R. solanacearum* infection on plant tissues. A. Tissue hydration. Fresh weight and dry weight were  
773 used to determine the proportion of water in healthy and infected tissues. Bars indicate standard deviation. B.  
774 Metabolic profile of tissues expressed in percentage of dry weight for starch and amino acids. The mean and  
775 standard deviation displayed were obtained after combining the acquired data of the two biological replicates  
776 (total of 12 samples for leaf, 10 for stem, 12 for root at each time point). In A. and B., healthy and infected  
777 plant data were compared by Wilcoxon-Mann-Whitney test (\*: p-value<0.05, \*\*: p-value<0.01).

778 **Figure 4**

779 Principal Component Analysis on metabolite concentrations from samples at different dpi.  
780 Representation of individual points (A) and the variables (B). Zero bacterial population corresponds  
781 to healthy plant samples. Data points at the top of the plot correspond to uninfected or low bacterial  
782 population samples while data points at the bottom correspond to high bacterial population samples.  
783 Principal component 1: 35% of variability. Principal component 2: 27% of variability. ETOH: ethanol,  
784 PUTR: putrescine, FUM: fumarate, SUC: sucrose, GLC: glucose.

785 **Figure 5**

786 Kinetics of metabolic contents in xylem sap of infected or healthy plants based on a total of 57 xylem  
787 sap samples obtained at different dpi. Healthy and infected plant data were compared by Wilcoxon-  
788 Mann-Whitney test (\*: p-value<0.05, \*\*: p-value<0.01).

789 **Figure 6**

790 Correlations between markers of the infection. For CFU per g of fresh weight, only data for which the  
791 counting was above  $10^7$  CFU per of fresh weight (corresponding to the “tipping point”) were included.

792 **Figure 7**

793 In vitro and in planta behavior of the *R. solanacearum* mutant strain GRS941 (carrying deletion in the  
794 sucrose, glucose and fructose transporter genes), compared to the wild-type strain GMI1000. Growth  
795 on minimal medium supplemented with sucrose (A) and glucose (B) as sole carbon source monitored  
796 in microplates with three independent biological replicates. Means and standard deviations are  
797 represented by the lines and colored areas, respectively. Bacterial density in planta (C) was determined  
798 on at least 9 plants per condition and per day, and plant transpiration (D) on at least 7 plants per  
799 condition and per day for infected WT/GRS941 (except 3 at 8 dpi) and at least 3 plants per day for  
800 healthy plants. Means are presented and bars indicate standard-deviation.

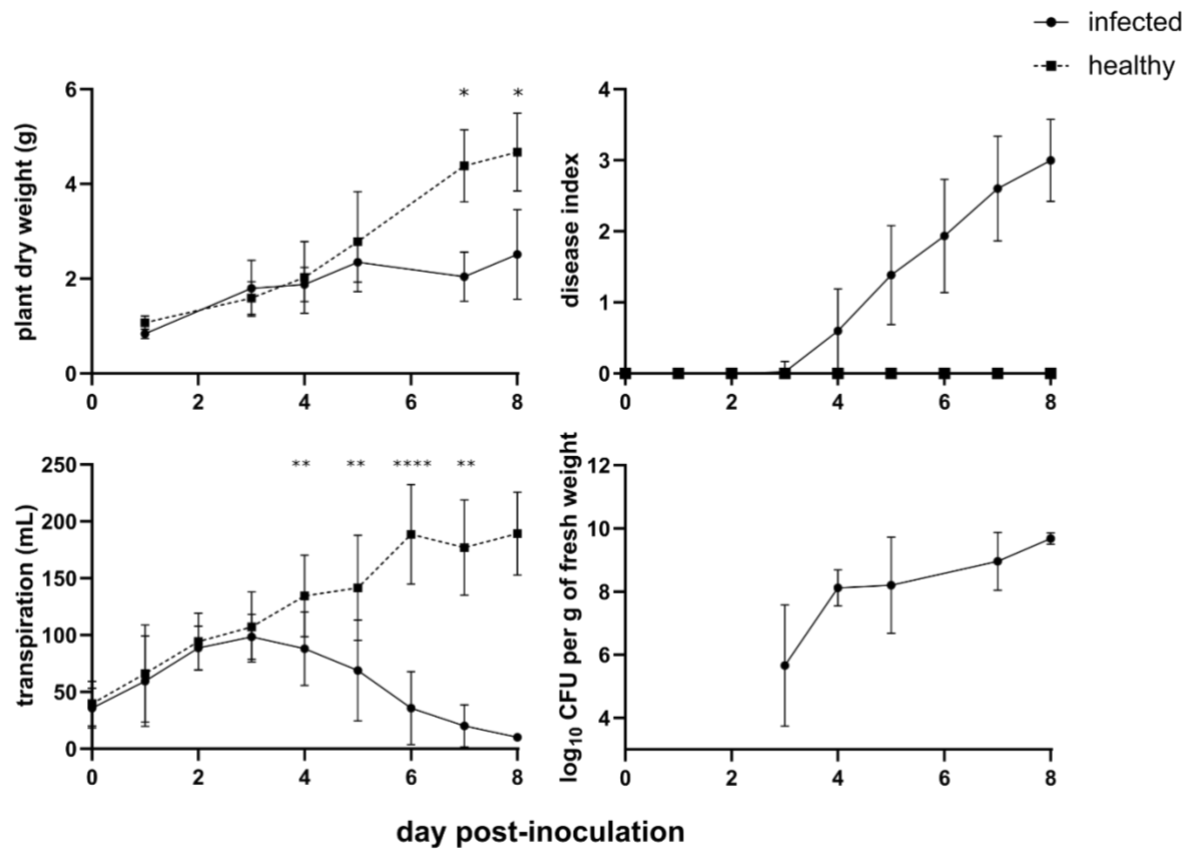


Figure 1

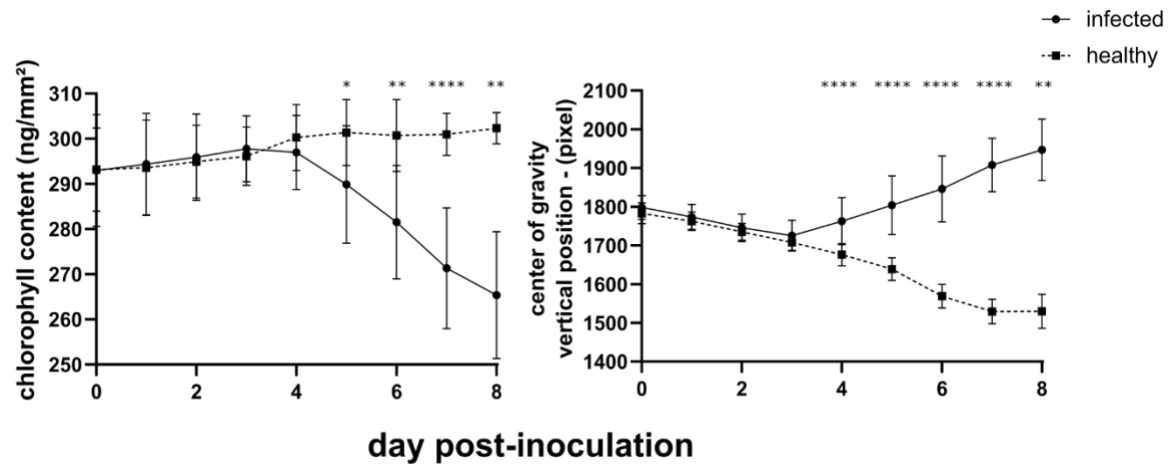


Figure 2

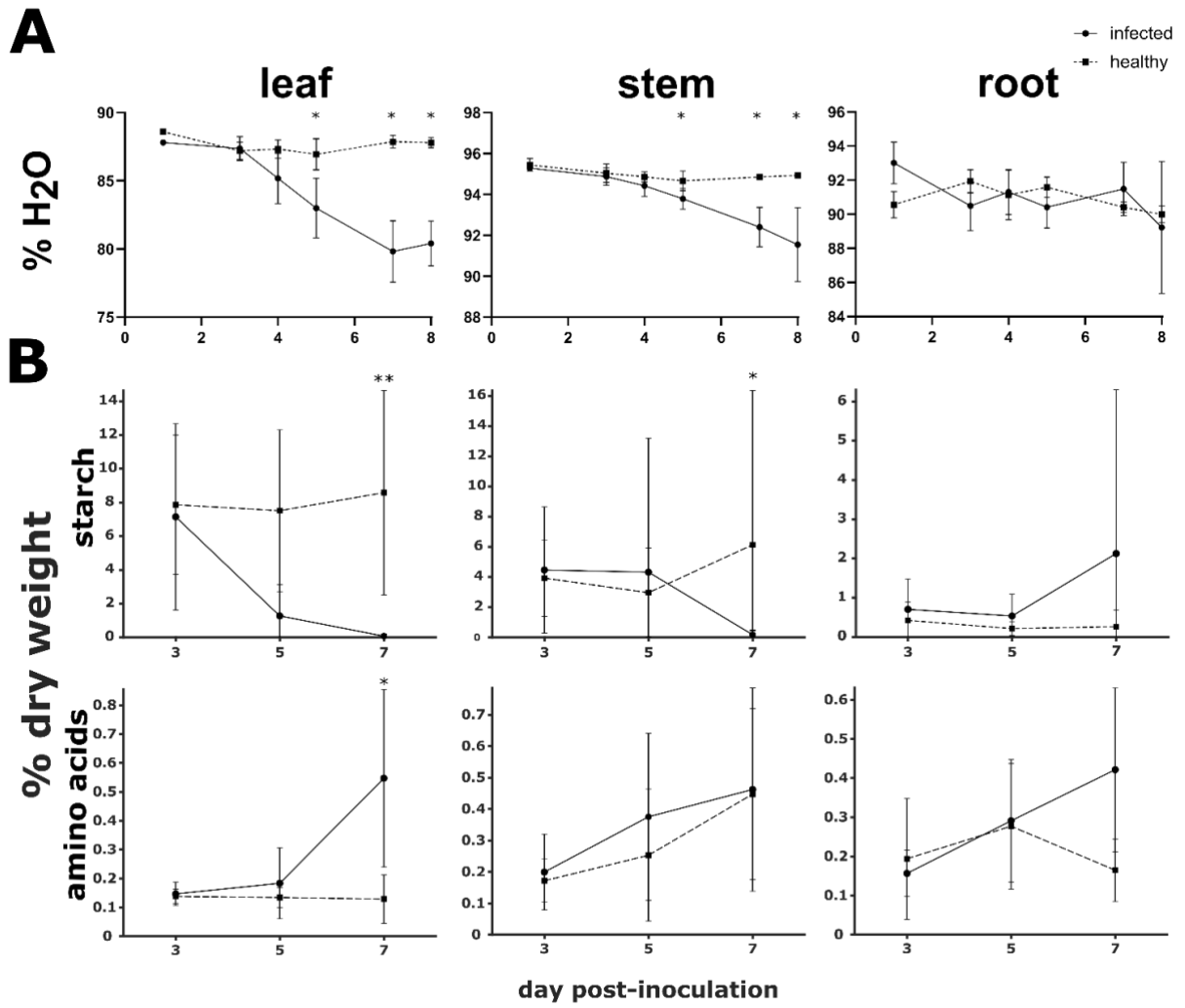


Figure 3

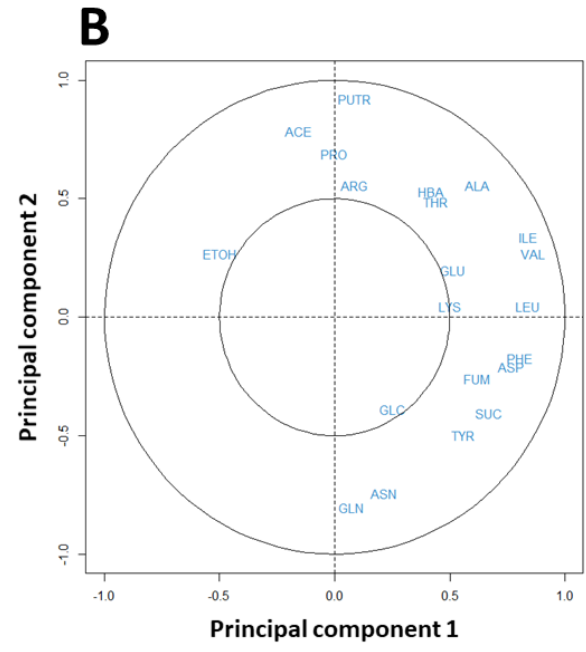
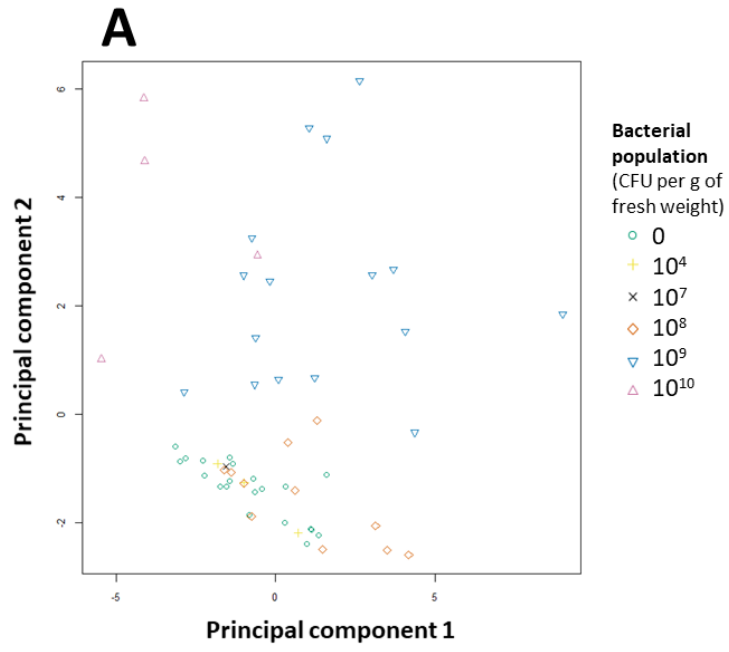


Figure 4

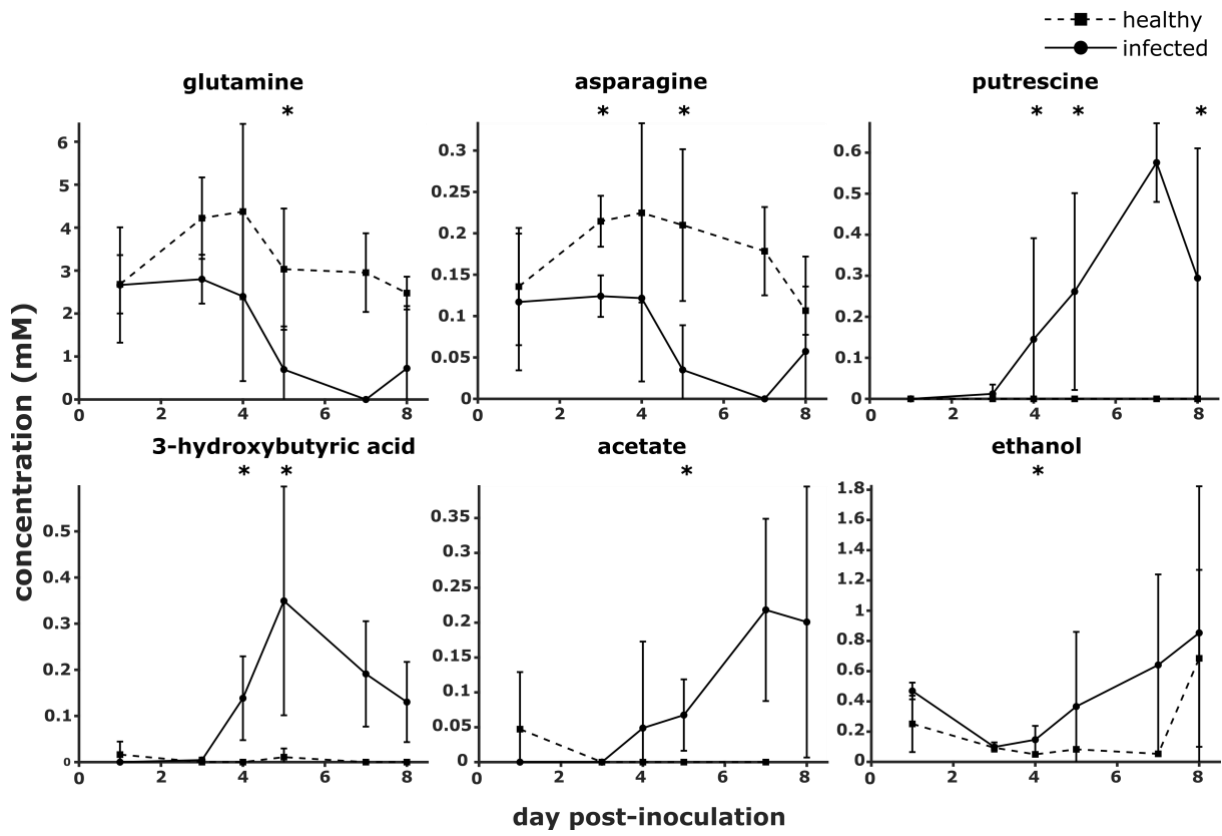


Figure 5

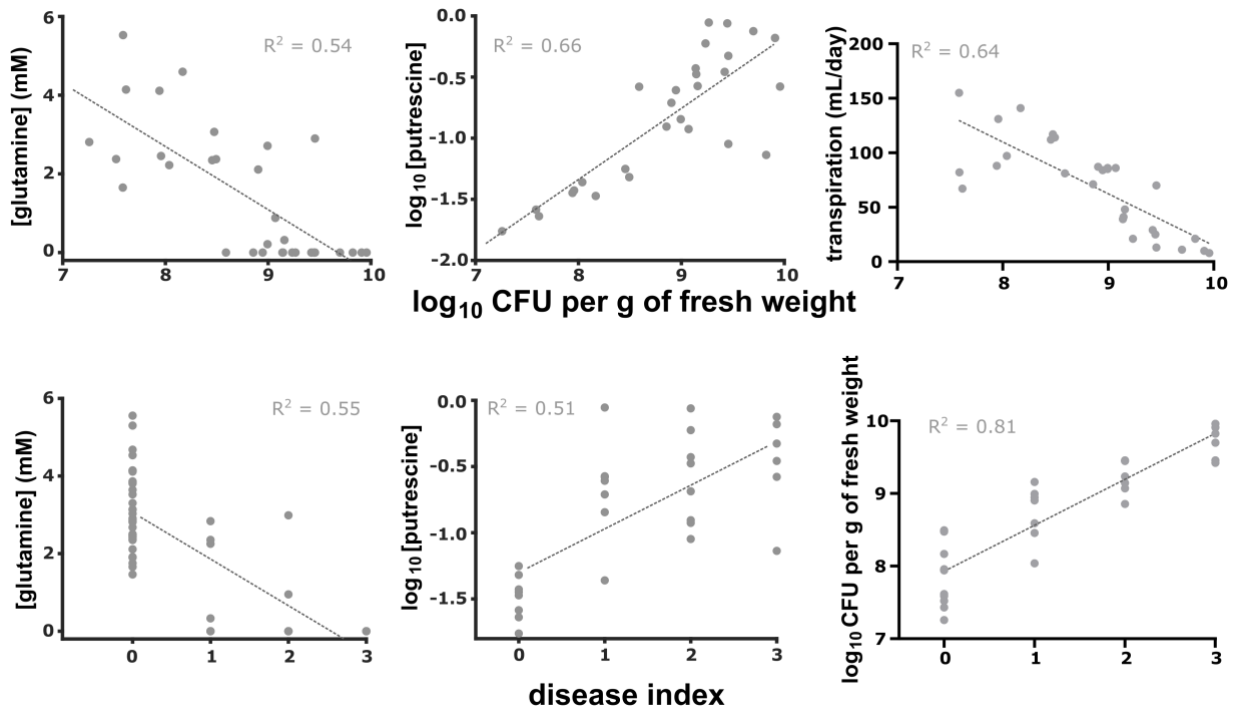


Figure 6

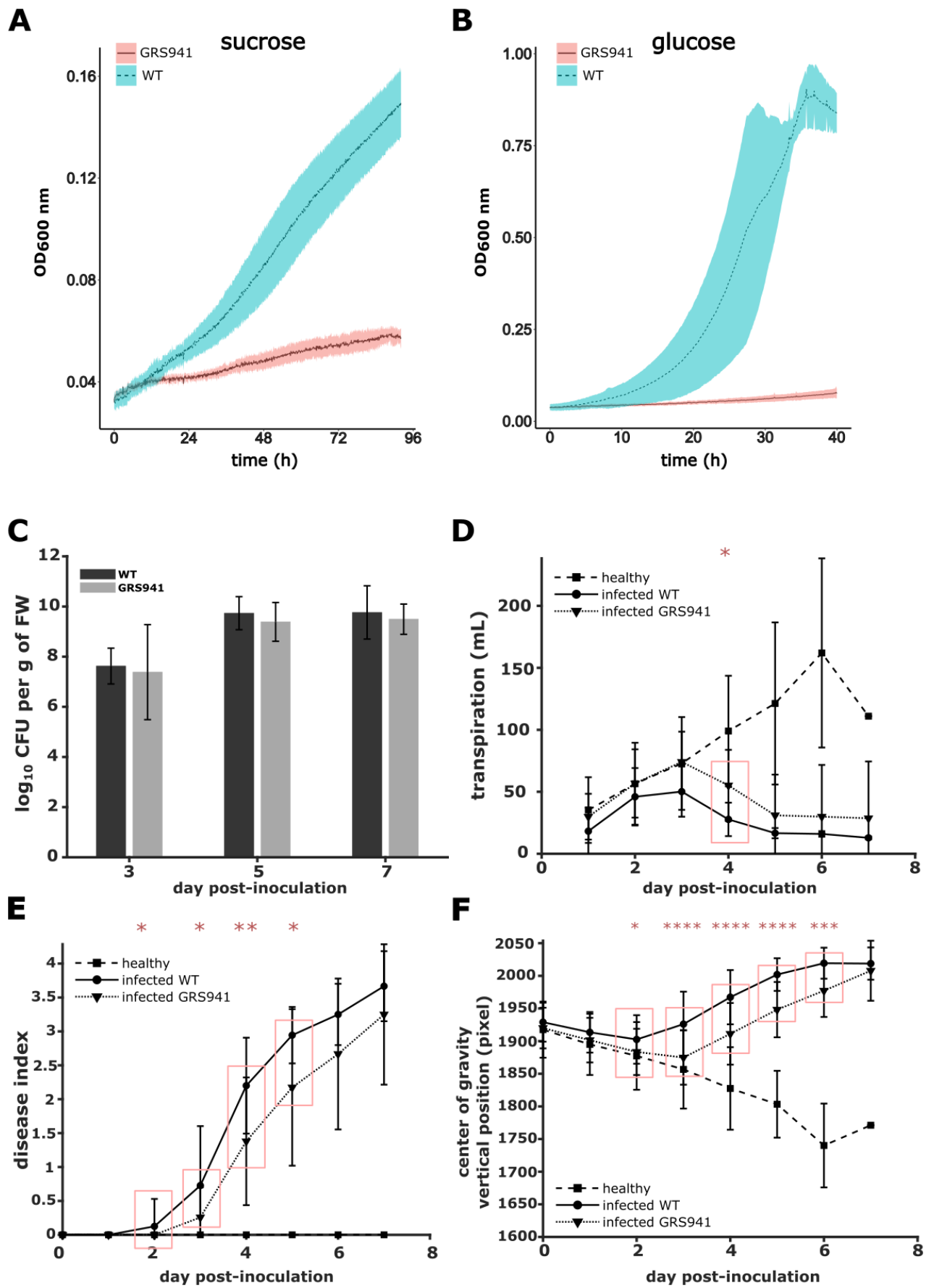


Figure 7

**Table 1. Xylem metabolite content and the impact of *R. solanacearum* infection**

<b>Metabolite</b>	<b>Concentration in healthy plant (mM)</b>	<b>Effect of the infection<sup>1</sup></b>	<b>Growth of <i>R. solanacearum</i> as sole carbon source<sup>2</sup></b>
glutamine	3.29 ± 1.25	decrease	+
asparagine	0.178 ± 0.074	decrease	+
tyrosine	0.022 ± 0.010	putative decrease	NA
glucose	0.010 ± 0.026	putative decrease	+
sucrose	0.028 ± 0.018	putative decrease	+
fumarate	0.004 ± 0.006	putative decrease	+
aspartate	0.015 ± 0.014	no effect	+
phenylalanine	0.035 ± 0.022	no effect	-
leucine	0.088 ± 0.029	no effect	-
lysine	0.123 ± 0.062	no effect	-
glutamic acid	0.020 ± 0.041	no effect	+
threonine	0.062 ± 0.019	putative increase	+
valine	0.083 ± 0.025	putative increase	+
proline	0.066 ± 0.033	putative increase	-
alanine	0.012 ± 0.007	putative increase	+
isoleucine	0.048 ± 0.015	putative increase	-
ethanol	0.203 ± 0.314	putative increase	NA
arginine	0.094 ± 0.051	putative increase	-
3-hydroxybutyric acid	0.005 ± 0.040	putative increase	+
acetate	0.008 ± 0.033	increase	+
putrescine	not detected	appearance	-

## Supplementary Figures and Tables

### Figure S1. Step-by-step segmentation pipeline.

Are represented the major steps of the segmentation process. The JSON script of this specific pipeline is available as supplementary file 1 and can be uploaded, run and modified using the IPSO-Phen software package available at Github [https://github.com/tpmp-inra/ipso\\_phen](https://github.com/tpmp-inra/ipso_phen).

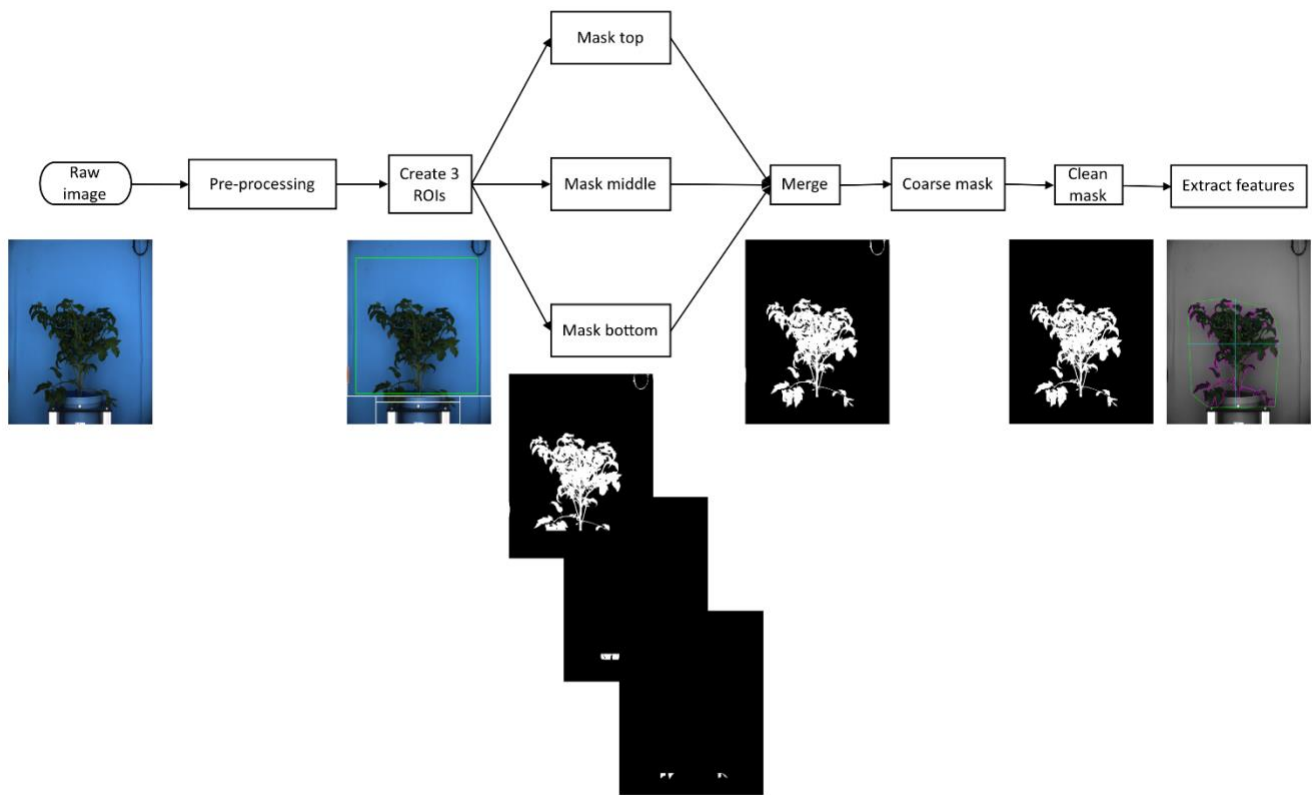


### Figure S2. The centroid-y trait (Cy).

The Centroid-y traitor "Cy" is the y coordinate of the center of gravity of the plant area (Cy is one of the traits extracted as a final step of the image analysis process (see Supplementary figure X0). The origin of the Y axis is set at the top of the image. Plant growth, as an upwards expansion, lowers the Cy value. Bacterial wilt, with leaves dropping and later decaying, increases the Cy value.



### Figure S3. Examples of Cy values on healthy and diseased plants.

Two distinctive plant images corresponding to disease index 0, or healthy, and diseased (DI=2, 3 or 4) are showed with their respective Cy values (in pixel).

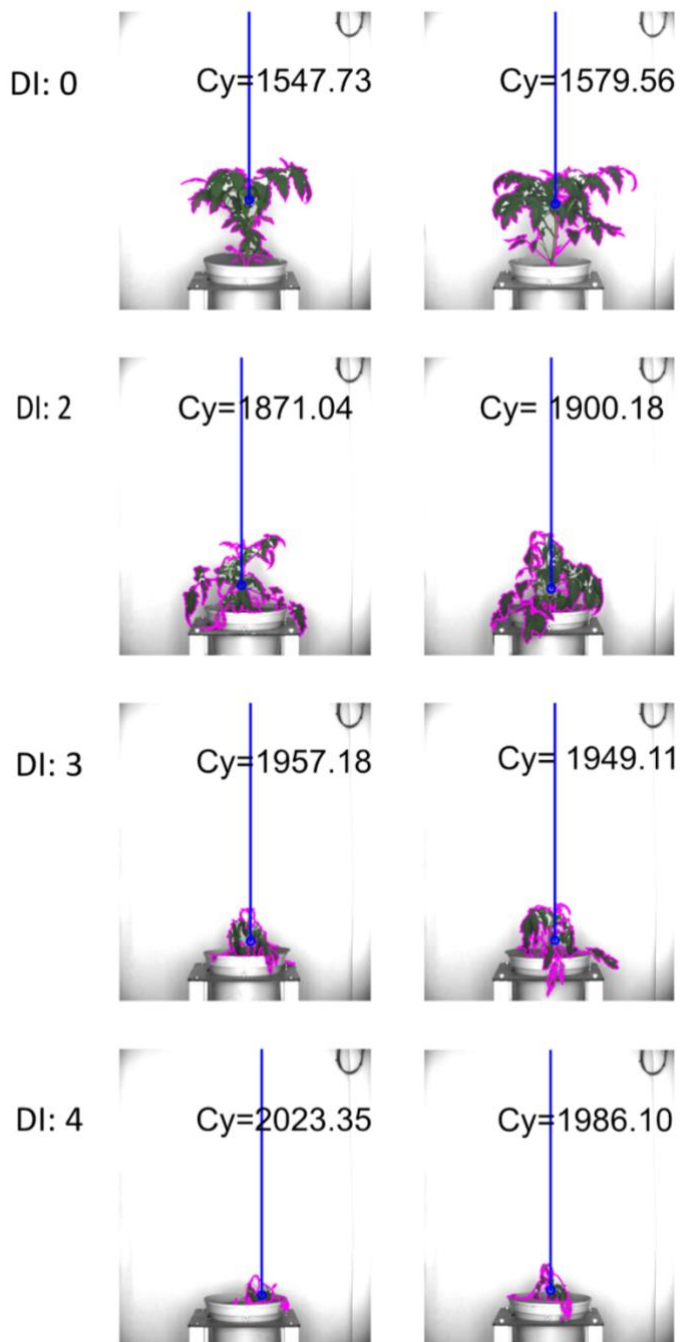


**Figure S4. Biological replicate of the physiological measurements.**

Impact of *R. solanacearum* colonization on plant physiology (dry weight/transpiration) and monitoring of disease kinetics (disease index), imaging parameters (chlorophyll/center of gravity position) and water content. Chlorophyll content was estimated through RGB values (automatic phenotyping) of plant images as described by Liang et al (Liang et al., 2017). Center of gravity position (vertical) was estimated through plant imaging (automatic phenotyping) with 0 pixel representing the top of the plant. The data presented are from an experiment on 90 plants with at least 3 plants per conditions at each sampling point. Fresh weight and dry weight were used to determine the proportion of water in healthy and infected tissues. Bars indicate standard deviation. Healthy and infected plant data were compared by Wilcoxon-Mann-Whitney test (\*: p-value<0.05, \*\*: p-value<0.01, \*\*\*: p-value<0.001, \*\*\*\*: p-value <0.0001).

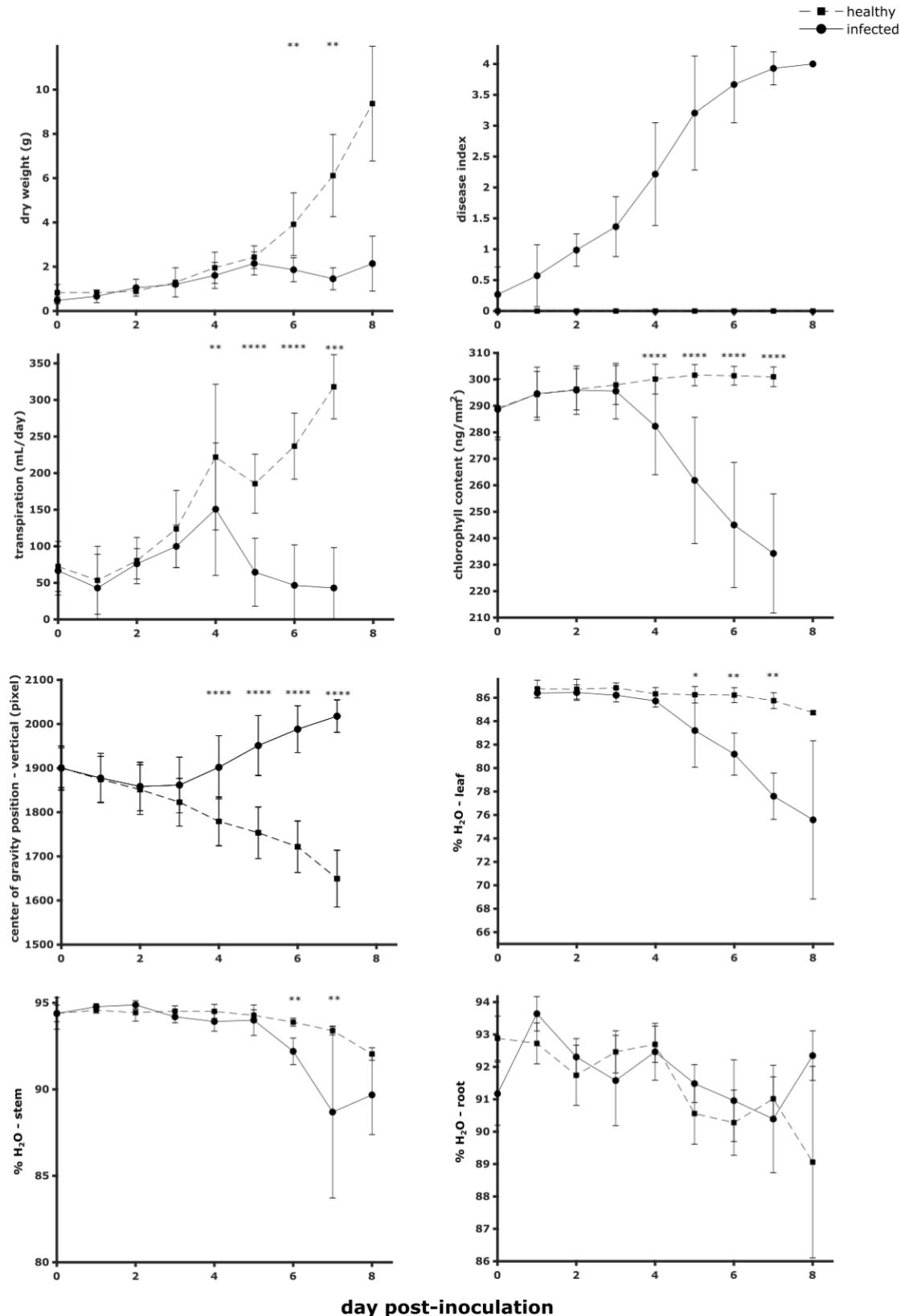


**Figure S5. Impact of *R. solanacearum* infection on plant tissues metabolic content.**

The mean and standard deviation displayed were obtained after combining the acquired data of the two biological replicates (total of 12 samples for leaf, 10 or 12 for stem, 12 for root at each time point). Healthy and infected plant data were compared by Wilcoxon-Mann-Whitney test (no significant change on the metabolites presented on this figure).

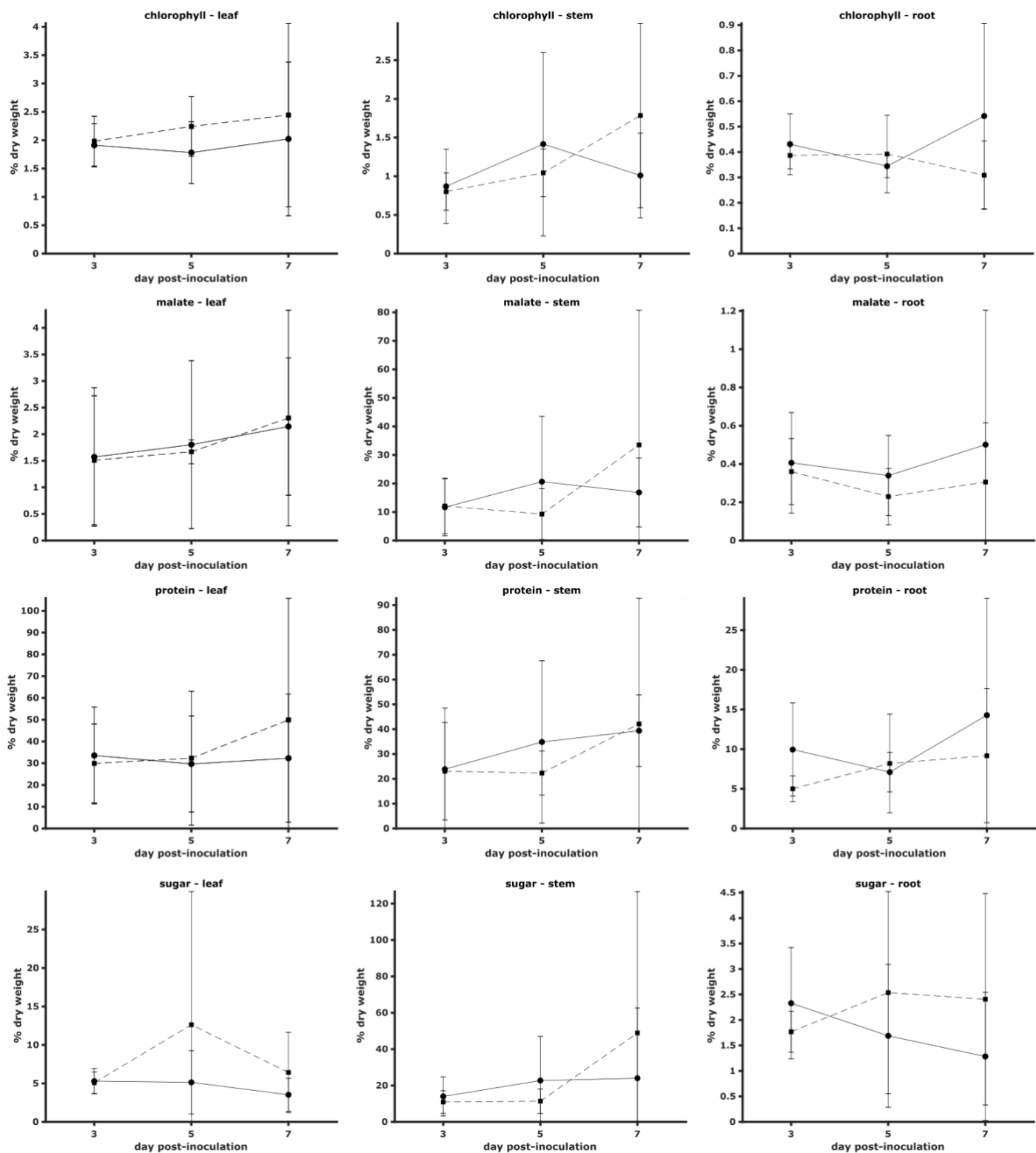


**Figure S6. PCA on the biological replicate data: experimental points (A) and variables (B).**

As CFU per gram of fresh weight data were not available, infection stage (ni: non-infected, ir\_bf\_3dpi: infected, sampling before or at 3dpi, ir\_af\_3dpi: infected, sampling after 3dpi) was mapped on the analyzed data. Similarly to the PCA presented in the Results section, glutamine are the compounds the most correlated with no infection or limited infection stage as it is oriented at the top left (B) which is associated with no or early infection. Oppositely, putrescine and acetate are at bottom right (B) which is associated with late infection. Other compounds associated with late infection include acetate, also noticed in the Results figure as associated with the infection. Other compounds appear to be associated with the infection so as fumarate but this association was not confirmed by the replicate presented in the Results figure.

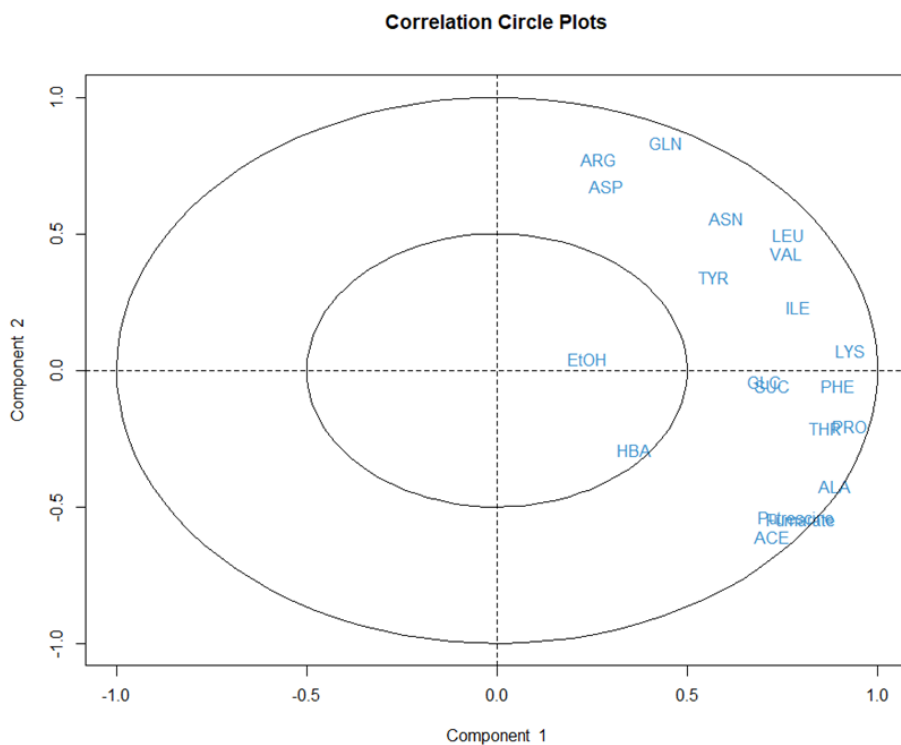
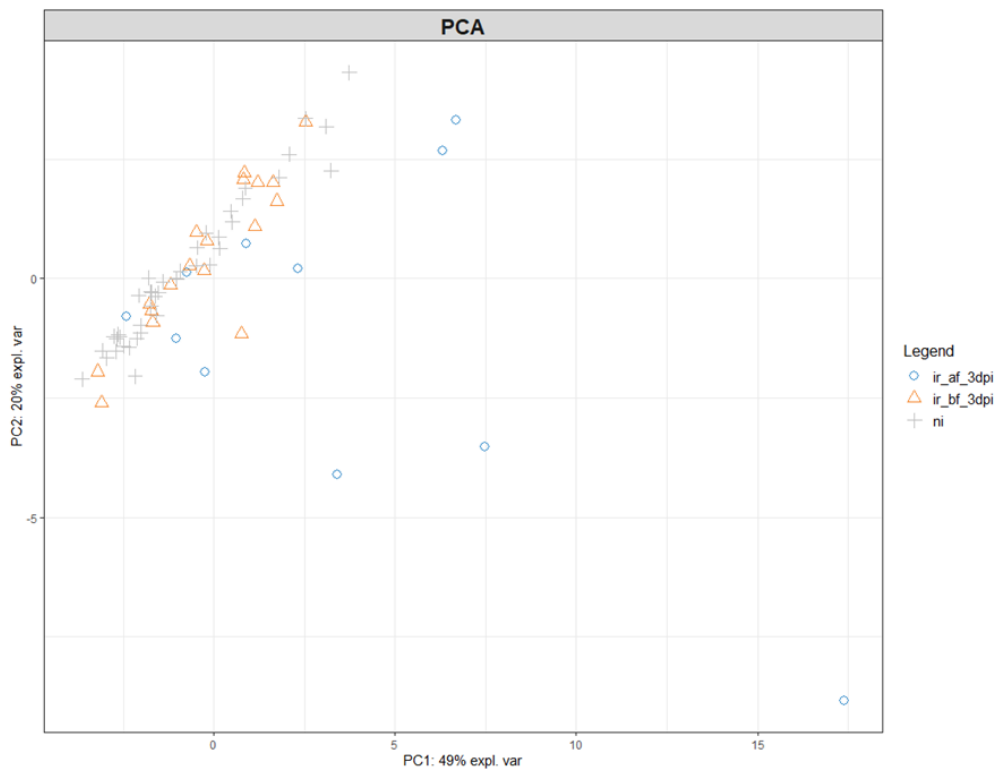


**Figure S7. Explained variance of the principal components.**

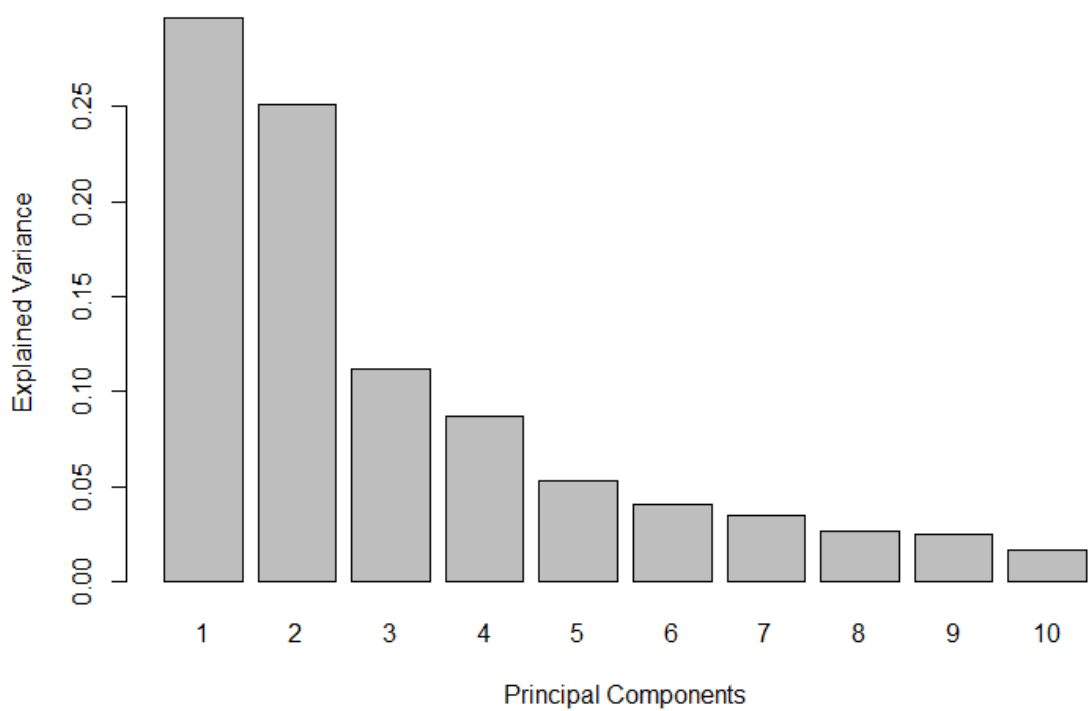
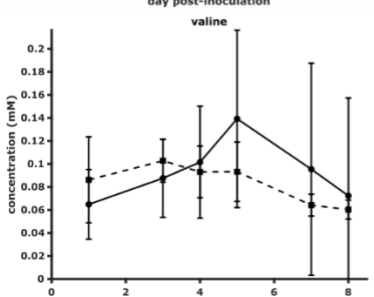
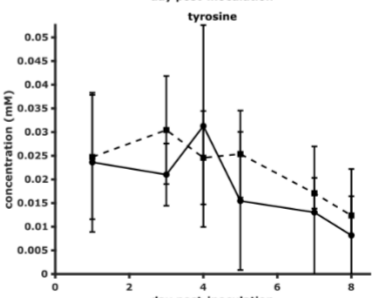
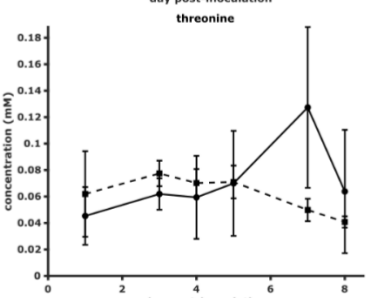
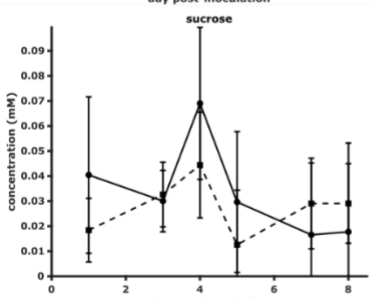
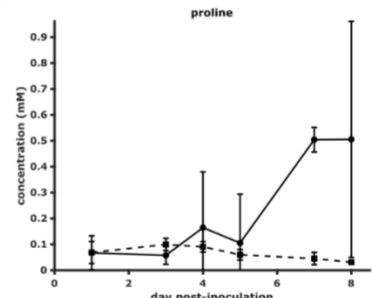
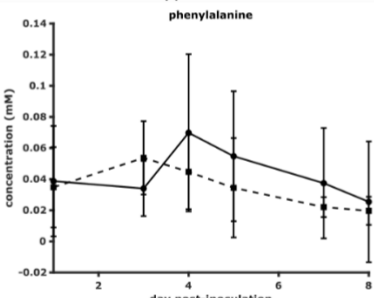
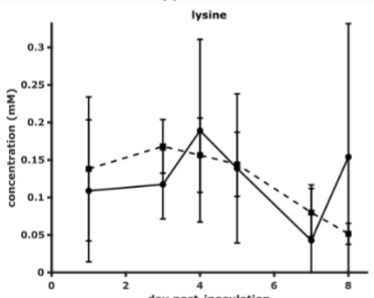
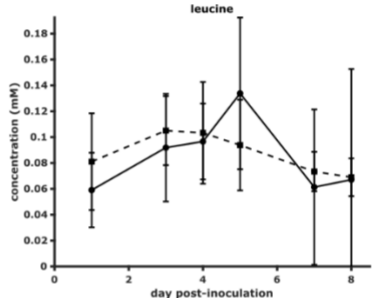
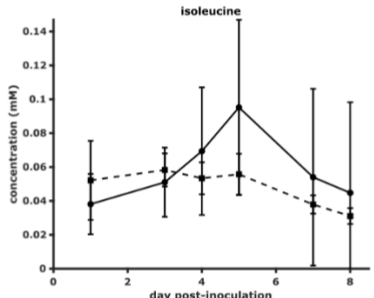
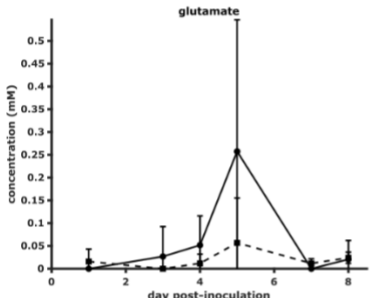
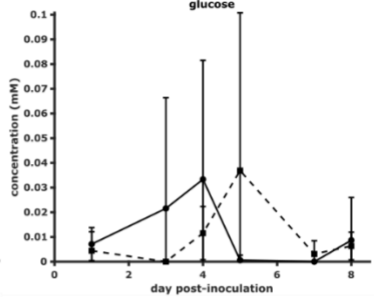
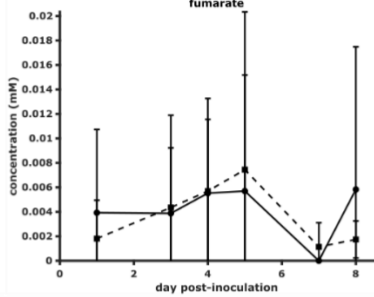
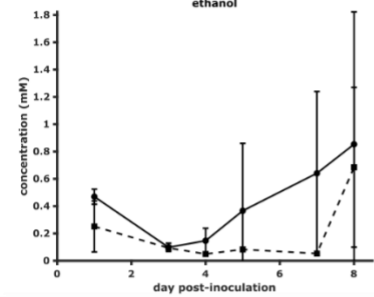
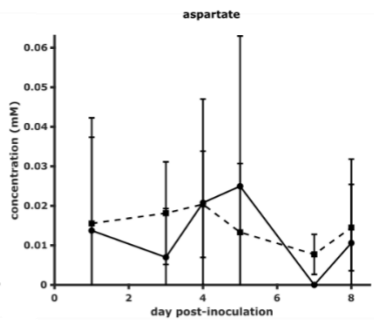
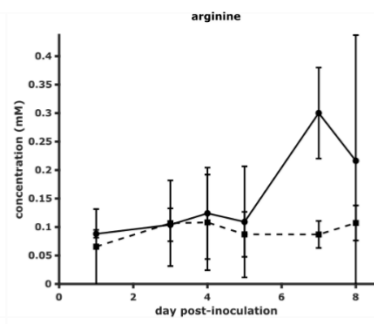
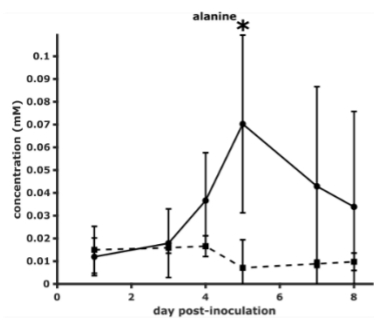


**Figure S8. Concentration profiles for alanine and other metabolites with non-statistically significant infection effect.**



— healthy  
— infected

**Fig S9. In vitro and in planta phenotyping of *R. solanacearum* triple mutant strain defective for glucose, sucrose and fructose assimilation.**

Growth on minimal medium supplemented with glutamine (A) and sucrose (B) as sole carbon source monitored in microplates with three independent biological replicates. Means and standard deviations are represented by the lines and colored areas, respectively. Plant dry weight (C, F) and bacterial population (H) were determined on at least 9 plants per condition and per day for infected WT/GRS941 (except 3 at 8 dpi for F) and at least 3 plants per condition and per day for healthy plants. Disease index, transpiration and chlorophyll content (D, E, G) were determined on at least 7 plants per condition and per day for infected WT/GRS941 (except 3 at 8 dpi for E, G) and at least 3 plants per day for healthy plants. E, F, G, H represent an independent experimental repeat, and C, D are complementary figures of the experiment presented in the results section of the article. Means are presented and bars indicate standard-deviation. Infection by wild-type (WT) and GRS941 strains data were compared by Wilcoxon-Mann-Whitney test (\*: p-value<0.05, \*\*: p-value<0.01).

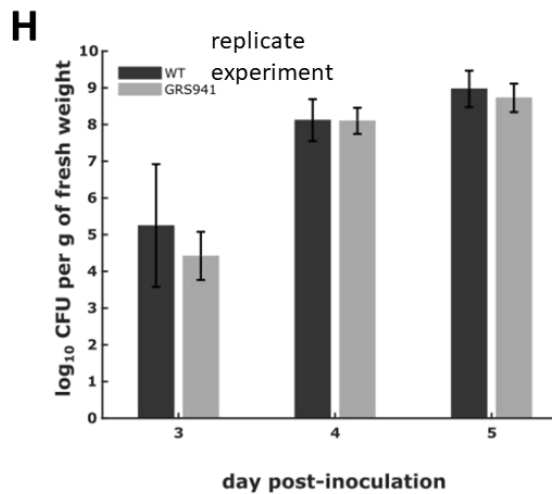
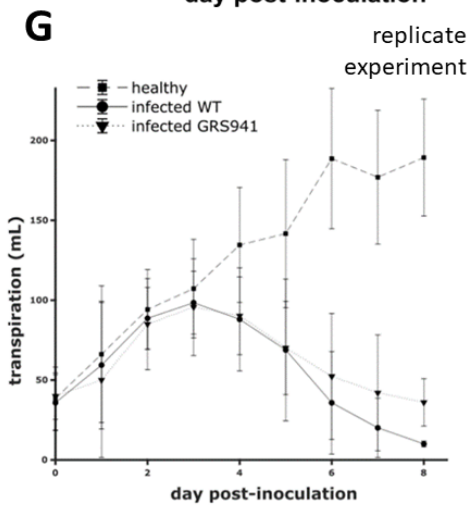
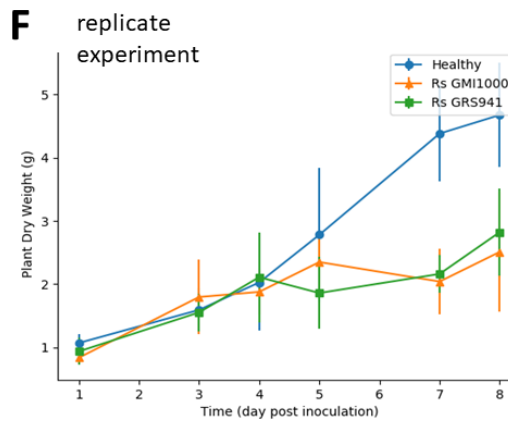
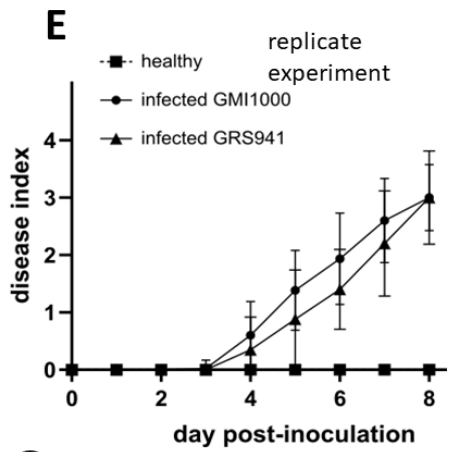
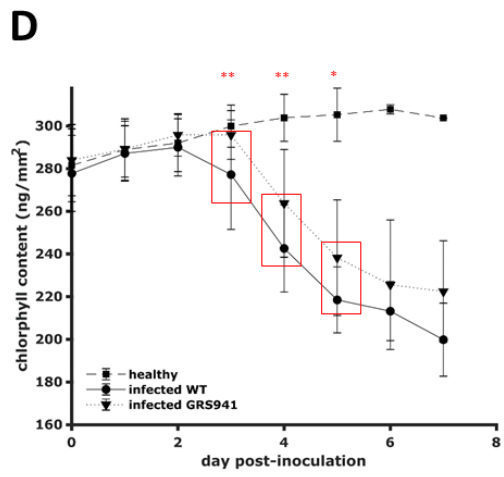
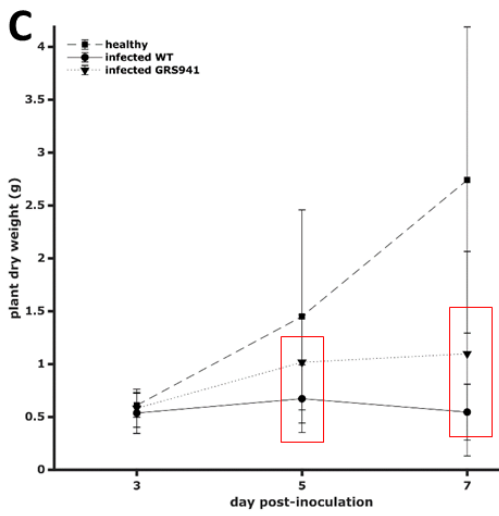
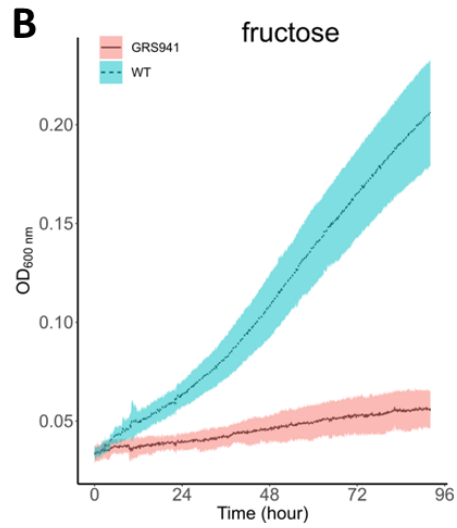
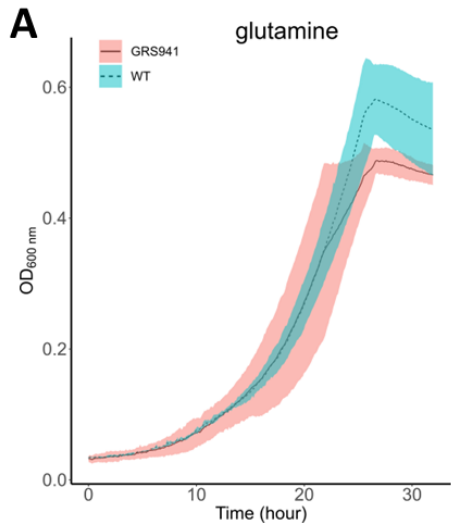
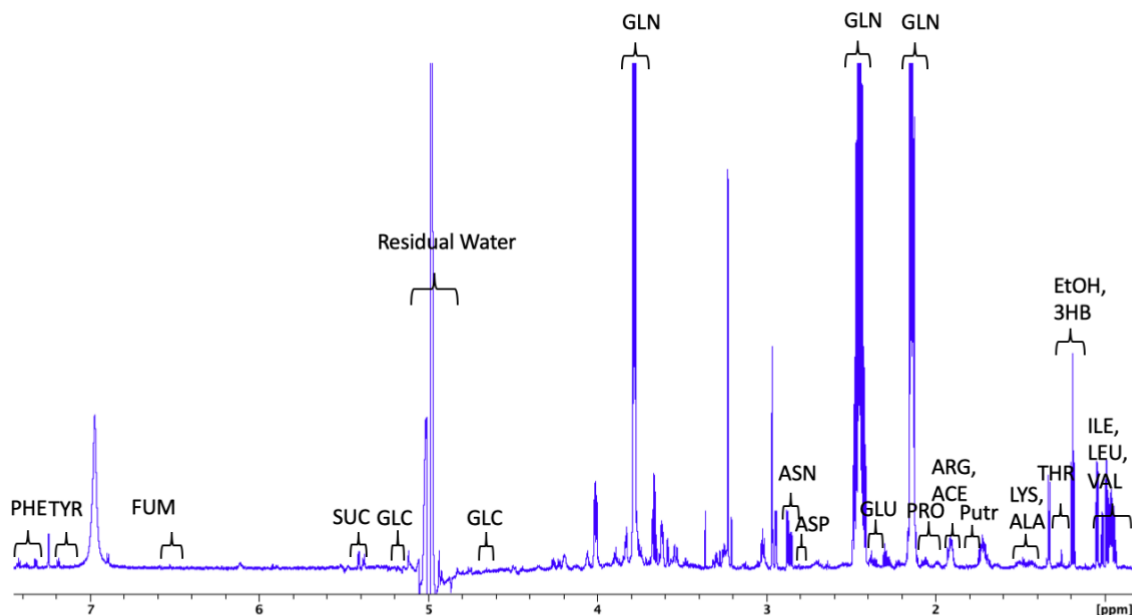


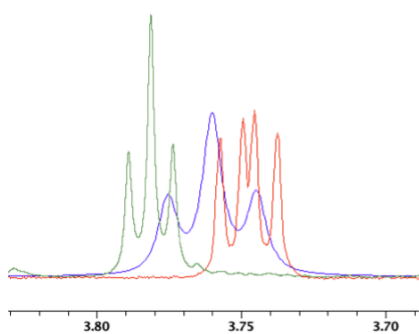
**Fig S10. NMR spectrum example.**

A. PHE: phenylalanine, TYR: tyrosine, SUC: sucrose, GLC: glucose, ASP: aspartate, ASN: asparagine, GLN: glutamine, GLU: Glutamate, PRO: proline, ARG: arginine, ACE: Acetate, Putr: Putrescine, LYS: lysine, ALA: Alanine, THR: threonine, EtOH: ethanol, 3HB: 3-hydroxybutyric acid, ILE: isoleucine, LEU: leucine, VAL: valine. B and C highlight the difference of spectrum aspects between glutamine and glutamate (or its conjugated acid glutamic acid), and a xylem sample with very few glutamate but high glutamine content: on B, the spectrum profile between 3.7 and 3.8 ppm is different (aspect and number of peaks) and on C, glutamine and glutamate profiles are very different: location and number of group of peaks.

**A**



**B**



**C**

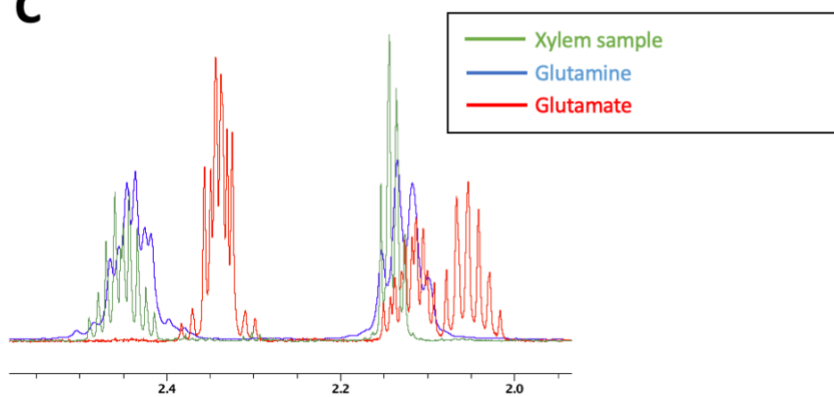


**Table S1. Biological replicate of the composition of non-infected xylem.**

<b>Metabolite</b>	<b>Concentration in healthy plant (mM)</b>
glutamine	3.259 ± 1.633
asparagine	0.143 ± 0.078
tyrosine	0.025 ± 0.007
glucose	0.031 ± 0.058
sucrose	0.070 ± 0.052
fumarate	0.002 ± 0.003
aspartate	0.017 ± 0.014
phenylalanine	0.029 ± 0.011
leucine	0.081 ± 0.029
valine	0.076 ± 0.026
proline	0.118 ± 0.058
lysine	0.163 ± 0.052
isoleucine	0.052 ± 0.017
arginine	0.132 ± 0.051
ethanol	0.771 ± 0.910
putrescine	not detected
threonine	0.058 ± 0.019
glutamate	not detected
acetate	not detected
3-hydroxybutyric acid	not detected
alanine	0.021 ± 0.007

**Table S2. Loading weights on the second component of the PCA. (update)**

<b>Metabolite</b>	<b>Loading weight</b>
PUTR	0.401
GLN	-0.350
ACE	0.339
ASN	-0.325
PRO	0.300
ARG	0.242
ALA	0.242
HBA	0.2309
TYR	-0.217
THR	0.212
SUC	-0.177
GLC	-0.169
ILE	0.146
ETOH	0.116
VAL	0.116
FUM	-0.113
ASP	-0.091

GLU	0.086
PHE	-0.075
LEU	0.020

## **Generation of *R. solanacearum* triple mutant strain defective for glucose, sucrose and fructose assimilation**

Strain GRS941 was engineered by cumulating deletions in the glucose transport operon (RSp1632-RSp1635), the sucrose assimilation operon (RSp1280-RSp1286) and the fructose transport operon (RSc2861-RSc2863).

An unmarked internal deletion in of the glucose transport operon ( $\Delta$ RSp1632-RSp1635) gene was created using the *sacB*-mediated counter selection system (Schäfer et al., 1994). Briefly, upstream (RSp1632) and downstream (RSp1635) regions were PCR amplified using the primer pairs 1632A/1632B and 1635C/1635D, respectively, and cloned into the *EcoRI-HindIII*-digested pk18mobsacB to generate pK18- $\Delta$ RSp1632/1635 (listed below). The circularized plasmid was recombined in strain GMI1000 through natural transformation (Perrier et al., 2018).

Kanamycin-resistant and sucrose-sensitive recombinant clones were first selected and in a second step, after overnight culture in BG medium (Plener et al., 2010), kanamycin-sensitive and sucrose-resistant clones were screened by PCR using the primer pair 1632A/1635D to identify a  $\Delta$ RSp1632-RSp1635 recombinant. The resulting mutant was named GRS903.

A deletion of the RSp1280-RSp1286 region was created by double recombination using a selectable antibiotic interposon cassette from pHP45 (Prentki & Krisch, 1984): upstream (RSp1286) and downstream (RSp1280) regions were PCR amplified using the primer pairs 1280R1 /1280Sc and ScrR-Xba/ScrR-R1, respectively, cloned in the pGEMT vector (Promega), and then the  $\Omega$  interposon was inserted in the unique *EcoRI* site. The resulting plasmid pSG804 was recombined in strain GRS903 through natural transformation as described above, and spectinomycin-resistant clones were selected and PCR-validated, yielding strain GRS936.

A deletion of the *fruBKA* operon (RSc2861-RSc2863) was created by double recombination using the selectable integrative plasmid pCM184 (Marx & Lindstrom, 2002): upstream (RSc2861) and downstream (RSc2863) regions were PCR amplified using the primer pairs fru-bgl-2/fru-nde-2 and fru-Sac2/fru-Sc1, respectively, and cloned in pCM184 as *BglIII-NdeI* and *SacII-SacI* inserts, respectively. This recombinant plasmid, pSG753, was recombined in strain GRS936 through natural transformation as described above, then gentamycin-resistant clones were selected and PCR-validated, yielding strain GRS941.

### List of oligonucleotides used in this study

1632A	GAATTCAGGAGACAGTCCATGGAGCTC
1632B	TCTAGATCAGCGCGCCGGTGGTG
1635C	TCTAGATCTCCGTCACGGGCATG
1635D	AAGCTTGACGATCATCTGCCACG
1280R1	GCCTGCTCACGCGCCCGGAGG
1280Sc	GAGCTCGCCCAACAAGTTCGAG
ScrR-Xba	TCTAGATCAATTCGTACACCAC
ScrR-R1	GAATTCAACCTCGGCGCTATTGC
fru-bgl-2	AGATCTGCTGGTGCGGCCGAACAGC
fru-nde-2	CATATGTGCTCGTCCGACTGCG
fru-Sac2	CTGGCGCGCATGCTGGACAG
fru-Sc1	GAGCTCGGCGTGTAGACCTGGC

## References

Marx CJ, Lidstrom ME (2002) Broad-host-range cre-lox system for antibiotic marker recycling in gram-negative bacteria. *Biotechniques* 33:1062-1067. doi: 10.2144/02335rr01.

Perrier A, Barberis P, Genin S (2018) Introduction of genetic material in *Ralstonia solanacearum* through natural transformation and conjugation. *Methods Mol Biol.* 1734:201-207. doi: 10.1007/978-1-4939-7604-1\_16.

Plener L, Manfredi P, Valls M, Genin S (2010) PrhG, a transcriptional regulator responding to growth conditions, is involved in the control of the type III secretion system regulon in *Ralstonia solanacearum*. *J Bacteriol.* 192:1011-1019. doi: 10.1128/JB.01189-09.

Prentki P, Krisch HM (1984) *In vitro* insertional mutagenesis with a selectable DNA fragment. *Gene* 29:303-313. doi: 10.1016/0378-1119(84)90059-3.

Schäfer A, Tauch A, Jäger W, Kalinowski J, Thierbach G, Pühler A (1994) Small mobilizable multi-purpose cloning vectors derived from the *Escherichia coli* plasmids pK18 and pK19: selection of defined deletions in the chromosome of *Corynebacterium glutamicum*. *Gene* 145: 69–73.